Chapter 3
Ruby Masers

Robert C. Clauss and James S. Shell

3.1 Introduction

Ruby masers are very low-noise pre-amplifiers used in the microwave receiving systems of the Deep Space Instrumentation Facility (DSIF) and the Deep Space Network (DSN) since 1960. Ruby masers are cryogenically cooled to temperatures below 5 kelvin (K) to achieve extremely low noise levels, and they are used near a focal point of large antennas for receiving signals from spacecraft exploring the Solar System.

Microwave amplification by stimulated emission of radiation (maser) is very different than the process in amplifying devices using a flow of electrons in a crystal (such as transistors) or using a beam of electrons in a vacuum (such as traveling wave tubes, klystrons, or triodes). The maser process may be quantified in terms of photons. A photon at microwave frequencies might be thought of as a particle or an amount of electromagnetic energy equal to hf where h is Planck's constant, 6.626×10^{-34} joule-seconds (J-s), and f is the frequency in hertz (Hz). For example, at 8.42 gigahertz (GHz), a frequency used for deep-space-to-Earth telecommunications, receiving one photon per second provides an amount of power equal to 5.58×10^{-24} watts (W) or –202.5 decibels referenced to milliwatts (dBm). The power level of one photon per second at 8.42 GHz is also equal to the noise power available from a 0.4041-K source in a 1-Hz bandwidth. 0.4041 K is the hf/k quantum noise at 8.42 GHz, where k is Boltzmann's constant (1.38×10^{-23} joule/kelvin (J/K)). The ultimate operating noise temperature lower limit of any linear receiving system is accepted as the quantum noise.

Ruby masers are the most sensitive and lowest noise microwave amplifiers used in the field, yet they are rugged and are not susceptible to the microscopic failures that sometimes occur in sub-micron junction devices. These characteristics of ruby masers result from the stimulated emission process used to amplify a signal. Stimulated emission is a photons-to-photons amplification process. The paramagnetic ruby crystal contains chromium ions, and these ions give the ruby a pink or red color. These ions each have three unpaired electrons. The intrinsic spin angular momentum of each of these electrons gives them the property of a magnetic moment. These three magnetic moments add together to form a larger effective permanent magnetic dipole moment. This permanent magnetic dipole moment associated with each chromium ion is referred to in the following text as a "spin." Spins in particular energy levels are excited by a process called pumping, the application of microwave energy to the ruby. Incoming signal photons stimulate the excited spins, which then drop from a higher energy level to a lower energy level, thereby emitting photons in-phase with, and in numbers proportional to, the stimulating signal photons. This photons-to-photons amplification process enables linear low-noise amplification while being quite immune to the generation of inter-modulation products when strong signals interfere with the reception of weak signals. Ruby masers can withstand input signal power levels of many watts without damage and are not subject to burnout or damage by voltage transients.

Cavity masers using ruby were developed at the Jet Propulsion Laboratory (JPL) at 960 megahertz (MHz) and at 2388 MHz. JPL's first cavity maser installed near the prime focal point on a 26-meter (m) diameter DSIF antenna at a Goldstone, California Deep Space Station (DSS) is shown in Fig. 3-1. The September 1960 occasion was JPL's first liquid helium transfer into an antenna-mounted maser at the DSS-11 "Pioneer" Site. The 960-MHz cavity maser was cooled to 4.2 K by liquid helium in an open-cycle dewar. The maser and the dewar were designed by Dr. Walter H. Higa and built by the group that he supervised at JPL. This first experimental field installation and testing period was followed by the installation of a 2388-MHz cavity maser in February 1961. The 2388-MHz maser was used to receive and amplify microwave radar echoes from the planet Venus [1]. Liquid helium was transferred on a daily basis at a height of about 24 m above the ground, from the fiber-glass bucket of the "cherry-picker" (High Ranger) seen in Fig. 3-1. Servicing the maser was exciting work, especially when the wind speed reached 18 meters per second (m/s) and buffeted the cherry-picker's bucket.

Several single-cavity 960-MHz (L-band) masers were built, some using open-cycle cooling and one cooled by a closed-cycle helium refrigerator [2]. A dual-cavity 2388-MHz maser was developed and used at the Goldstone DSS-13 "Venus" Site to receive radar echoes from Venus and Mars [3]. Traveling-wave maser (TWM) systems were developed for use at various S-band frequencies

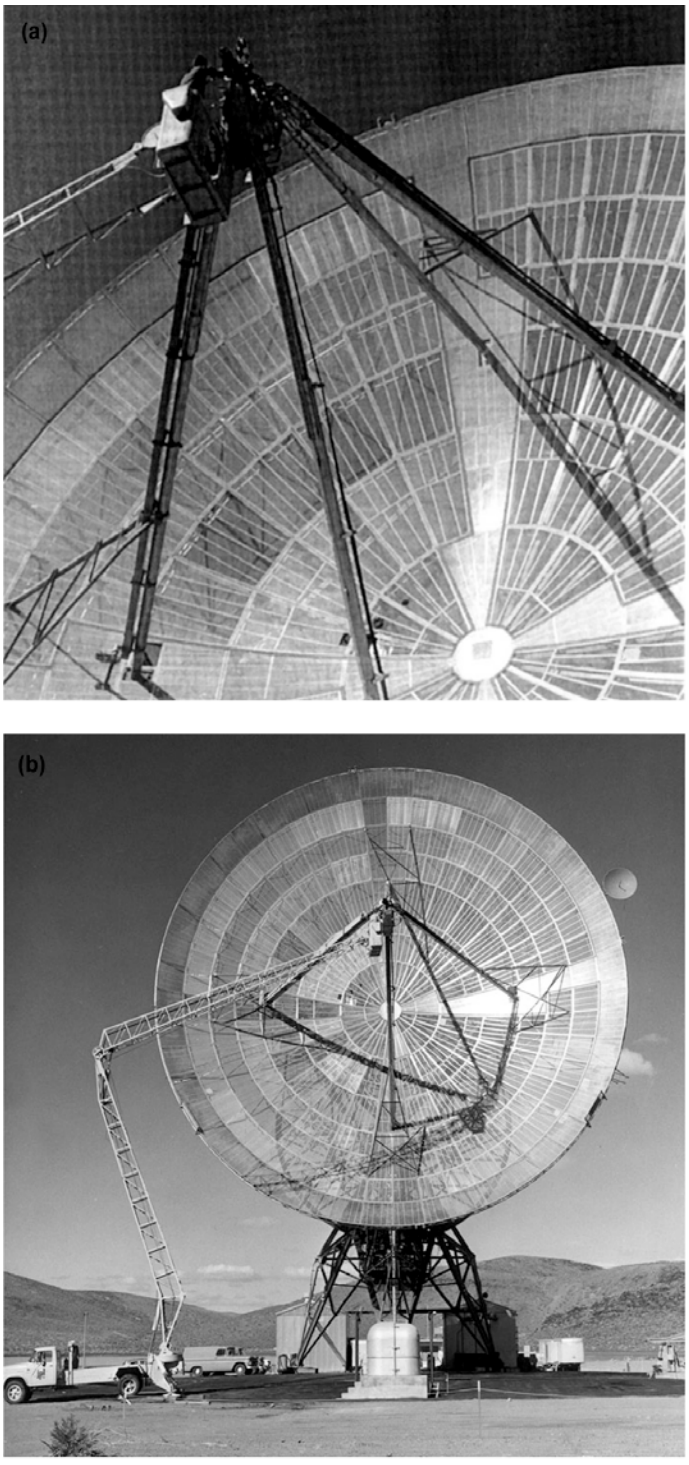

Fig. 3-1. Liquid helium transfer. Including (a) manual transfer of liquid helium at DSS-11 and (b) zoom-out view of cherry picker (high ranger) in use for liquid-helium transfer.

between 2200 MHz and 2400 MHz, X-band frequencies between 7600 MHz and 8900 MHz, and at Ku-band frequencies between 14.3 GHz and 16.3 GHz [4]. K-band reflected-wave maser (RWM) systems were developed for radio astronomy applications at frequencies between 19 GHz and 26.5 GHz. The TWMs and RWMs all operated in closed-cycle refrigerators (CCRs) at temperatures near 4.5 K. An RWM was developed to cover the 31.8-GHz to 32.3-GHz deep-space-to-Earth frequency allocation at Ka-band. A 33.7-GHz two-cavity maser was developed and used at DSS-13 for the Ka-band link experiment with the Mars Observer spacecraft [5].

Table 3-1 lists the ruby masers built for and used in the DSN. Twenty-seven Block III S-band TWMs were implemented. 90 ruby masers were used in the DSN since 1960. CCRs and other key parts were reused as they became available, after replacement by later model masers. R&D masers were built and used in the field, usually on the research antenna at DSS-13 and in the research (radar) cone at DSS-14, to evaluate the long-term performance prior to operational spacecraft tracking commitments. Occasionally R&D masers were installed and used to support and enhance missions following spacecraft problems that affected the communications link.

3.2 Ruby Properties

The pink ruby crystal used in maser amplifiers is about 99.95 percent aluminum oxide (Al_2O_3) with approximately 0.05 percent chromium oxide (Cr_2O_3). The paramagnetic Cr^{3+} ions occupy some of the sites normally occupied by the Al^{3+} ions. Ruby used in the early cavity masers and TWMs was grown by the flame-fusion process and usually contained multiple crystal orientations and variations in the chromium concentration (doping gradients). Inspection and selection of the ruby to find pieces of adequate size and quality were needed. This inspection process was done in polarized light, using a cross-polarized lens to view the flaws in the ruby. Superior quality ruby was developed primarily for laser applications by the Union Carbide Corporation using the Czochralski process. Czochralski ruby first became available for maser applications in 1966.

Ruby is a hard, stable, rugged low-microwave-loss, and high-dielectric-strength crystalline material that can be cut or ground to precise dimensions with diamond tools. The dielectric constant is anisotropic, varying from 11.54 in the direction parallel to the axis of symmetry (c-axis) to 9.34 in the direction perpendicular to the c-axis. The dielectric loss tangent is very low (< 0.0001) and not measurable in ruby-filled cavities or in the slow-wave structures of TWMs. Ruby survives repeated thermal cycling from ambient temperatures above 300 K to cryogenic temperatures below 5 K. The thermal conductivity of ruby is about 1 watt per centimeter-kelvin (W/cm-K) at 4 K and is adequate for

Table 3-1. DSN ruby maser history.

Time in Use[3]	Frequency (GHz)	Maser Type	Bath Temp. (K)	Gain (dB)	Bandwidth (MHz)	Noise Temp. (K)	Quantity[3]
1960–65	0.96	Cavity	4.2	20	0.75	17–30[1]	5
1961	2.388	Cavity	4.2	20	2.5	25	1
1962–63	2.388	Dual cavity	4.2	34	2.5	18	1
1963–66	2.388	R&D TWM	4.5	40	12	8	1
1964–66	8.45	Multiple cavity	4.2	33	17	18	1
1964–71	2.295	Block I S-band TWM	4.5	33	17	9–15[1]	6
1965–71	2.27–2.30	Block II S-band TWM	4.5	35	17–30	9–15[1]	8
1966–68	8.37–8.52	R&D TWM	4.5	30–45	17	18–23[1]	1
1966–74	2.24–2.42	R&D TWM	4.5	27–50	16	4–6[1]	3
1970–89	2.285	Block III S-band TWM	4.5	45	40	4–6[1]	27
1970–72	7.6–8.9	R&D TWM	4.5	30–42	17	7–13[1]	1
1971–80	14.3–16.3	R&D TWM	4.5	30–48	17	8–13[1]	1
1973–89	7.8–8.7	R&D TWM	4.5	45	17–20	7–11[1]	1
1974–now	2.25–2.4	R&D TWM	4.5	30–50	15–30	2–4[1]	1
1975–89	8.42	Block I X-band TWM	4.5	45	40	5–10[1]	12
1979–now	2.285	Block IV S-band TWM	4.5	45	40	2	4
1980–now	8.45	Block II X-band TWM	4.5	40	100	3–4.5[1]	9
1981–95	18–25	RWM	4.5	30	100–300	12	3
1986–95	2.21–2.32	Block V S-band TWM	4.5	35–45	70	3–5	2
1992–now	8.475	R&D TWM	1.6	34	100	1.9[2]	1
1992–94	33.3–34.0	Dual cavity	1.5	25	85	4–6[1,2]	1

[1] Range (varies across tuning range, from unit to unit, or due to measurement uncertainty)

[2] At the feedhorn aperture

[3] Quantities and time in use dates were obtained via personal communications with D. Hofhine of the Goldstone DSCC, and M. Loria of DSMS Operations.

maser applications. For comparison, thermal conductivity of 50–50 lead-tin soft solder is about 0.15 W/cm-K at 4 K, and the thermal conductivity of electrolytic-tough-pitch copper is about 4 W/cm-K at 4 K.

3.3 Spin Resonance, the Applied Magnetic Field, Ruby Orientation, the Low-Temperature Requirement, and Excitation

The energy of the spins in ruby varies with the intensity and orientation of a biasing magnetic field with respect to the c-axis of the ruby. Two different orientations of ruby are used in JPL masers, depending upon the signal frequency. The "90-degree" orientation used at L-band, S-band, X-band, and Ku-band is discussed here. The "54.7-degree" orientation is discussed later in the sections describing masers at X-band and higher frequencies. The direction of the c-axis can be determined in polarized light.

The four ground-state microwave spin levels that occur are called paramagnetic levels or Zeeman levels. The magnetic field strength and orientation used for an S-band maser at a frequency near 2.4 GHz is given here, for example. A magnetic field strength of 0.25 tesla (T) (2500 gauss (G)) is applied to the ruby in a direction that is perpendicular to the c-axis. This is called the 90-degree orientation. The energy spacings (h*f*) between the four ground-state energy levels in ruby under these conditions were given in terms of frequency (*f*). The spacing between these levels is: 1–2 = 2.398 GHz, 1–3 = 12.887 GHz, and 1–4 = 24.444 GHz. Slightly more accurate values are available today, but these values used during the development of masers at JPL between 1959 and 1990 are sufficiently accurate.

The example above uses values from the Appendix, "Ruby energy levels and transition-probability matrix elements," in *Microwave Solid-State Masers* [6]. Chang and Siegman published "Characteristics of ruby for maser applications," in 1958 [7]. Professor Siegman's thorough history and explanation of masers, together with his acknowledgment and descriptions of the research work and publications of many in the maser field are not duplicated here. His book contains a large volume of material about masers, including much that was produced by many workers who shared their knowledge generously. The extensive material published about maser theory and techniques between 1956 and 1964 was most helpful, aiding in the timely development of ruby masers at JPL for the Deep Space Network. Professor Siegman's book is recommended to those interested in the history of masers, and for the detailed theory that leads to a better understanding of masers.

Spin resonance absorption in ruby-filled cavity or waveguide may be observed with a microwave spectrometer as a function of frequency and an applied magnetic field. Absorption of power occurs when signals are applied at frequencies corresponding to the difference in frequency between energy levels.

The resonance absorption line-width of single crystal ruby with about 0.05-percent Cr^{3+} in a uniform magnetic field is about 55 MHz. This value, plus or minus 10 percent, is independent of temperature and has been measured at many different frequencies between 2 GHz and 40 GHz. The S-band example above gives the three frequencies between the 1–2, 1–3, and 1–4 levels. Spin resonance absorption also occurs at frequencies corresponding to the energy differences between levels 2–3 (10.489 GHz), 2–4 (22.046 GHz), and 3–4 (11.557 GHz). The magnitude of the absorption depends upon the ratio of spins in the various levels and is very weak at room temperature. At thermal equilibrium, the ratio of spins in an upper state (N_i) with respect to the lower state (N_j) is an exponential function of energy difference and temperature. The Boltzmann expression gives this ratio and the results show the need for physically cooling the maser material to low cryogenic temperatures.

$$\frac{N_i}{N_j} = e^{-\frac{\mathrm{h} f_{ij}}{\mathrm{k} T}} \tag{3.3-1}$$

where h is Planck's constant, f_{ij} is the frequency difference between levels i and j in hertz, k is Boltzmann's constant, and T is the thermodynamic (bath) temperature in kelvins.

Consider the difference in the ratios of spins in levels 2 and 1 (N_2 / N_1) in the S-band example above at various temperatures. When $T = 300$ K, $\mathrm{h}f_{12} / \mathrm{k}T = 3.8362 \times 10^{-4}$ and the ratio is 0.99962. The two spin populations are almost equal, and the absorption measured with a microwave spectrometer is very weak. As the temperature is lowered from 300 K to 100 K, 20 K, 10 K, 4.5 K, 2.5 K and 1.5 K, the ratios (N_2 / N_1) decrease from 0.99962 to 0.99885, 0.99426, 0.98856, 0.97475, 0.95501, and 0.92615, respectively.

Whether large or small, when the ratio of spins in the upper level to the lower level is less than 1, signal absorption occurs. Amplification by stimulated emission depends on a population inversion where the ratio is greater than 1. The low temperature advantage occurs in both the absorption case and the emission case.

Inversion of the spin population between energy levels 1 and 2 requires the use of an additional level or levels. The Boltzmann expression shows that, in thermal equilibrium, the number of spins in each level decreases from the lowest to the highest level. The example of the S-band maser at a temperature of 4.5 K is used here. The ratio of spins in level 2 to level 1 is 0.97475. The ratio of spins in level 3 to level 1 is 0.87159. The ratio of spins in level 4 to level 1 is 0.77051. Application of a sufficiently strong pump signal at the frequencies of either 12.887 GHz or 24.444 GHz will equalize the spin

populations of levels 1 and 3, or 1 and 4. Either of these frequencies can be used as the "pump" frequency to excite the spin system, to create a population inversion.

The total number of spins in ruby with slightly more than 0.05 percent Cr^{3+} is about 2.5×10^{19} per cubic centimeter (cc). The S-band cavity maser used as an example has a ruby volume exceeding 1 cc. The actual dimensions are not important for this excitation example. The ratios of the spin densities (in spins per cubic centimeter) in one level to another level are important. Consider x number of spins in level 1 for the thermal equilibrium un-pumped case. The spins in levels 1, 2, 3, and 4 are x, 0.97475 x, 0.87159 x, and 0.77051 x, for a total spin population of 3.61685 x. The fraction of spins in each level are, level 1 = 0.27648, level 2 = 0.26950, level 3 = 0.24098, and level 4 = 0.21304. The spin density values for each of the levels are level 1 = 6.9120×10^{18}, level 2 = 6.7375×10^{18}, level 3 = 6.0245×10^{18}, and level 4 = 5.3260×10^{18}. The level 2 spin density value is 1.745×10^{17} less than level 1. Equalizing the spins in levels 1 and 4 reduces the spin density in level 1 from 6.9120×10^{18} to 6.1190×10^{18} [$(6.9120 \times 10^{18} + 5.3260 \times 10^{18})/2$]. The number of spins in level 2 and level 3 remain unchanged. The ratio of spins in level 2 to level 1 is now 1.1011, a ratio greater than one. The population inversion between levels 2 and 1, resulting from pumping between levels 1 and 4, provides 6.185×10^{17} more spins per cubic centimeter (cc) in level 2 than in level 1.

Emission of the 6.185×10^{17} excess spins in level 2 in a 0.02-microsecond (μs) time period suggests that a pulse from a 1-cc ruby crystal at 2398 MHz could reach 9.8×10^{-7} J (49 W for 2×10^{-8} seconds). This pulse is capable of damaging a transistor amplifier following the maser, as demonstrated in the laboratory during an unfortunate pulse-amplification experiment. A spin-relaxation time of 50 ms for ruby at 4.2 K suggests this pulse amplification process could be repeated at a rate of 20 times per second, resulting with an equivalent continuous power level of about 20 microwatts (–17 dBm). This is about twice the maximum emission level of a –20-dBm signal observed to be available from an S-band TWM. Such a TWM, with low-level signal net gain of 45 dB shows about 1 dB of gain compression when the input signal reaches –84 dBm (the maser output signal is –40 dBm). The maser gain decreases gradually as the input signal strength is increased until the input reaches –20 dBm. At this point, the maser is a unity-gain amplifier. Increasing the input signal above –20 dBm causes the TWM to become a passive attenuator.

Pumping the S-band maser between levels 1 and 4 in the example above appears to give much better maser performance than would be achieved by pumping between levels 1 and 3. Measurements show that this is not the case. This simple example does not include other considerations that affect the performance of masers. Various parameters, including the spin-lattice relaxation time, inversion ratios, transition probabilities, and the filling factor must be considered.

3.4 Spin-Lattice Relaxation Time, Inversion Ratios, Transition Probabilities, the Filling Factor, and Magnetic Q

It is expedient to use the spin-lattice relaxation times measured and published by others. For ruby, in the microwave region at a temperature of 4.2 K, these times are of the order of 0.050 seconds. Below 5 K, these times are roughly inversely proportional to temperature [6, p. 225]. It seems reasonable to expect the spin relaxation times for the various levels to be roughly equal. Optimum spin relaxation times provide higher inversion ratios than equal spin relaxation times. Inversion ratios also vary in accordance with the pumping scheme used. Siegman, [6, p. 292 and 293] mentions four multiple pumped schemes and gives inversion ratio equations for the single-pumping three-level scheme and the multiple-pumping push-pull scheme. The signal frequency (f_s) and the pump frequency (f_p) in the three-level scheme used at S-band results in inversion ratios of $(f_p / f_s) - 1$ for the case of optimum spin-relaxation times and $(f_p / 2 f_s) - 1$ for the case of equal spin relaxation times.

The actual inversion ratio is determined by measuring the signal frequency amplification (the electronic gain in decibels) in the pumped case and dividing it by the signal frequency spin system absorption (in decibels) in the un-pumped case. Spin system absorption and inversion ratios were measured experimentally for many ruby orientations at many different frequencies and for other potential maser materials as well. The measurements at JPL used either a small dielectric resonator in waveguide, in the reflection mode, or the slow-wave structure of a TWM operating in the transmission mode. The use of a dielectric resonator in the reflection mode gives reliable results when the absorption values are a few decibels and amplification values are modest, between a few decibels and 10 dB. Regenerative gain can give gain values higher than those caused by the actual inversion ratio and must be avoided during the inversion ratio measurements.

Our most accurate inversion ratio measurements for S-band used a TWM at 2295 MHz. The pump frequencies used were 12.710 GHz (1–3 transition) and 24.086 GHz (1–4 transition). These calculated inversion ratios are shown in Table 3-2, along with the measured inversion ratios.

The absolute accuracy of the inversion ratio measurement could not resolve the ratio to better than ±0.1, but the difference between the two measurements observed by alternately turning the pump sources on and off was more precise, and it clearly showed the slight advantage for the higher frequency pump. Pump power was adequate for complete maser saturation in both cases.

The results of these inversion ratio tests at 2295 MHz suggest one of three possibilities: (1) The measured inversion ratio of 4.5 is close to the calculated

Table 3-2. Inversion ratios for a 2295-MHz TWM.

Pump Frequency (GHz)	Calculated Inversion Ratios for		Measured Inversion Ratios
	Equal Spin Relaxation Times	Optimum Spin Relaxation Times	
12.710	1.77	4.54	4.5
24.086	4.25	9.5	4.6

value of 4.54 for the 12.710-GHz pump case with optimum spin relaxation times; (2) The measured ratio of 4.6 is less than half of the value of 9.5 calculated for the 24.086-GHz pump case with optimum spin relaxation times, but is not far above the calculated value of 4.25 for the 24.086 pump case with equal spin relaxation times. One might assume that the spin relaxation time from level 3 to level 2 is much shorter than the spin relaxation time from level 2 to level 1, the optimum case. One might also assume that the spin relaxation time from level 4 to level 2 is slightly shorter than the spin relaxation time from level 2 to level 1. Both assumptions could explain the results; (3) There might also be a third explanation for the apparent almost ideal inversion ratio obtained with the 12.710-GHz pump, one that includes nearly equal spin relaxation times. The spacing between level 3 and level 4 is 11.376 GHz, the difference in frequency between the 24.086 GHz pump frequency and the 12.710 frequency. This 3–4 transition has an extremely strong transition probability. The action of the 12.710-GHz pump, that pumps spins from level 1 up to level 3, may also elevate spins from level 3 to level 4, achieving an effect similar to pumping from level 1 to level 4 directly with 24.086 GHz. This process, called push-push pumping, will receive more attention in the X-band maser section of this chapter.

Transition probabilities for the various ruby orientations and for various magnetic field strengths are given in the appendix to Professor Siegman's book [6] that was mentioned earlier. Transition probabilities are directional, having a maximum-probability direction and a zero-probability direction called the null direction. In the case of the 90-degree (deg) orientation where the applied magnetic field is perpendicular to the c-axis, we find the null direction for the signal frequency transition is in the direction of the applied magnetic field. Any microwave magnetic field components in this direction will not interact with the spin system. The c-axis direction is the direction of maximum signal transition probability for the 90-deg orientation in ruby and the radio frequency (RF) magnetic field components in this direction will have the maximum interaction with the spin system at frequencies below 15 GHz. A third direction, perpendicular to the plane determined by the c-axis direction and the applied magnetic field direction, has a transition probability less than the maximum transition probability at frequencies below 15 GHz, being about one-tenth the maximum transition probability at 2295 MHz.

A ruby-filled coaxial cavity, similar to the one used at the 2388-MHz maser for the Venus radar in 1961, is used to give a visual example of the RF magnetic field interaction with the ruby spin system. Figure 3-2 shows the cavity in which the center conductor is shorted at the bottom and open ¼ wavelength from the bottom. The ruby cylinder has a 1.9-cm outside diameter with a 0.636-cm hole through the center, and it is approximately 1 cm in length. The outside diameter of the ruby fits tightly into a copper outer conductor, and the center conductor of the ¼-wavelength resonator is a close fit in the 0.636-cm hole. The center conductor extends slightly beyond the ruby, and this length is adjusted to obtain resonance at the signal frequency. The signal is coupled through the capacitor formed by a sapphire sphere located between the center conductor of the ¼-wavelength cavity and the open-ended center conductor of the coaxial transmission line shown in part above the maser. The orientation of the sapphire sphere affects the capacitive coupling to the cavity

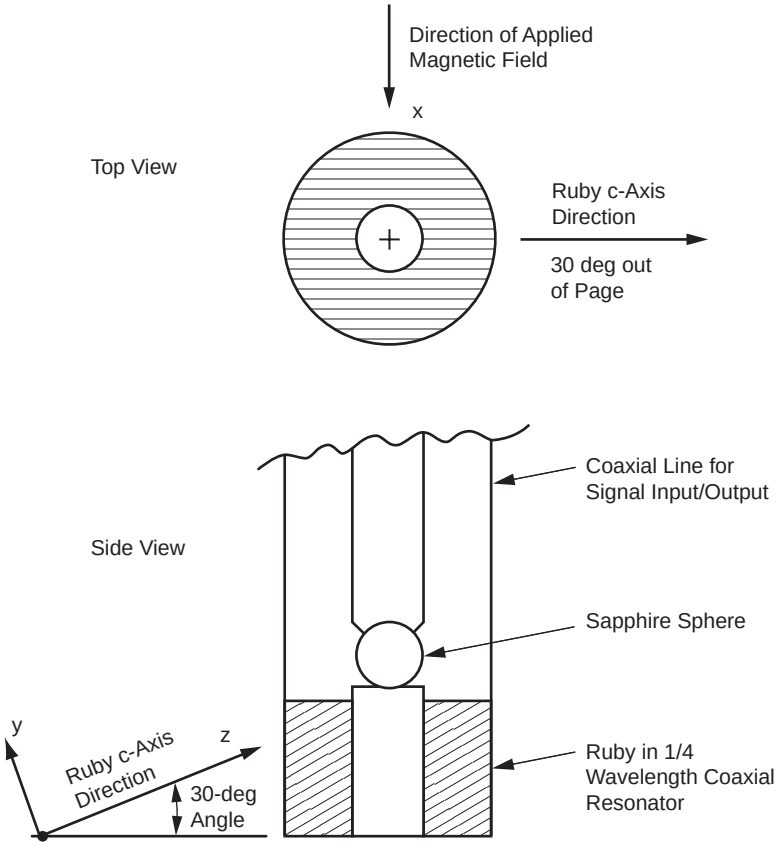

Fig. 3-2. Ruby-filled 2388-MHz coaxial cavity maser. (The ruby c-axis is also the z-axis of maximum transition probability.)

and the resulting cavity resonant frequency; this is caused by the anisotropy of the sapphire's dielectric constant. Figure 3-3 shows a cross-sectional view of the coaxial cavity maser and dewar system.

The ruby cavity is located inside of a liquid helium dewar for cooling to 4.2 K. The ruby c-axis direction in the cavity forms a 60-deg angle with the direction of the center conductor as shown in Fig. 3-2. The applied magnetic field of about 0.25 T comes from a magnet located at room temperature, outside the dewar. The coaxial transmission line and ruby-filled cavity is rotated until the ruby c-axis direction is perpendicular to the direction of the magnetic field.

The directional transition probabilities in "ruby energy levels and transition-probability matrix elements" [6] are given in terms of alpha, beta, and gamma, corresponding to the x, y, and z directions in Fig. 3-2. In this case the x-direction, being the same direction as the applied magnetic field direction, is the null-direction. The c-axis direction is the z-direction of maximum transition probability and is the direction of greatest importance. The projection of the z-direction into the plane of the circular RF magnetic field determines the resultant efficiency or filling factor of about 0.43 for the signal frequency interaction with the spin system. The projection of the y-direction into the plane of the circular RF magnetic field is such that the interaction between the spin system and the RF magnetic field in that part of the cavity is very low, having little affect on amplification. The transition probability in the y-direction is about 1/10 of the transition probability in the z direction. If the c-axis of the ruby had been perpendicular to the direction of the center conductor, in the plane of the signal frequency RF magnetic field, the filling factor would have been near the maximum value of 0.5. The combination of the circular RF magnetic field pattern and the linear c-axis direction results in a 0.5 maximum filling factor when the entire cavity is filled with ruby. The important considerations in determining the filling factor are the placement of the active material in the regions where the RF magnetic field is strong, and a parallel alignment of the RF magnetic field direction with respect to the direction of maximum transition probability.

The filling factor, inversion ratio, and transition probability values all affect the maser's amplifying ability. These, combined with the physical temperature, the maser material's spin density, the number of energy levels, the frequency, and the maser material 55-MHz line-width, determine the magnetic Q value (Q_m). Q_m is used to calculate the gain of a maser, be it a cavity maser, a traveling-wave maser, or a reflected wave maser. A simplified approximation for the Q_m of ruby with 0.053-percent Cr^{3+} (a spin density of 2.5×10^{19} spins/cm^3) at frequencies below 10 GHz and temperatures above 4 K is

$$Q_m \approx \frac{(141) \cdot T}{f I \sigma^2 \eta} \tag{3.4-1}$$

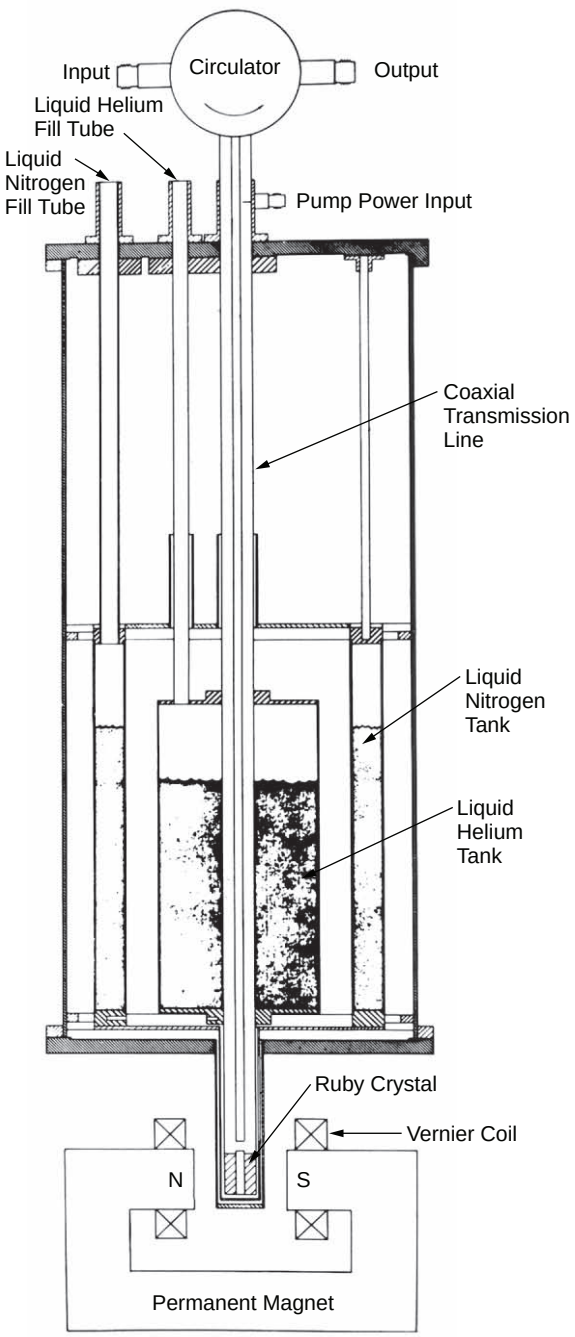

Fig. 3-3. Cross-section of a coaxial cavity maser and dewar system.

where

T = the thermodynamic temperature, K

f = the frequency, GHz

I = the inversion ratio

σ^2 = the maximum value of the transition probability matrix elements, and

η = the filling factor

A Q_m of 71.6 is calculated using I = 4.3, $\sigma^2 = 1.6$, and $\eta = 0.5$ for the 2.398-GHz cavity maser at 0.25 T (2500 G) and at 4.2 K. Siegman indicates [6, p. 255] that the approximation $hf / kT << 1$ holds for this estimate of magnetic Q.

The use of the actual spin density difference (ΔN) between the two levels adjacent to the signal transition results in a magnetic Q calculation that is not dependent upon $hf / kT << 1$.

$$Q_m = \frac{4.22 \times 10^{19}}{(\Delta N) I \sigma^2 \eta} \tag{3.4-2}$$

The thermal equilibrium (un-pumped) spin density values for the 2.398-GHz cavity maser example at 4.2 K are level 1 = 6.95925×10^{18}, level 2 = 6.77125×10^{18}, level 3 = 6.00625×10^{18}, level 4 = 5.26325×10^{18}. $\Delta N = 1.88 \times 10^{17}$.

$$Q_m = \frac{4.22 \times 10^{19}}{1.88 \cdot 10^{17} \cdot (4.3) \cdot (1.6) \cdot (0.5)} = 65.2 \tag{3.4-3}$$

The Q_m values of 71.6 for the approximation and 65.2 for the more exact calculation of the S-band example are within 10 percent of each other, suggesting that the low-frequency high-temperature approximation ($hf / kT << 1$) is useful in some cases.

An example of a maser at a higher frequency and a lower temperature uses the 33.7-GHz maser at 1.5 K. Here $I = 2$, $\sigma^2 = 1$, and $\eta = 0.5$. Using the approximation from Eq. (3.4-1) for this case, we calculate a Q_m of 6.26. The energy level distribution for the 33.7-GHz maser is calculated using the equation for the Boltzmann distribution. The frequencies corresponding to these levels are 1–2 = 35.92 GHz, 1–3 = 69.62 GHz, and 1–4 = 105.54 GHz. The signal frequency transition is the 2–3 transition at 33.70 GHz. The thermal equilibrium (un-pumped) spin density values for the 33.70-GHz cavity maser at 1.5 K are: level 1 = 1.7137×10^{19}, level 2 = 5.4303×10^{18}, level

$3 = 1.8473 \times 10^{18}$, and level $4 = 5.8850 \times 10^{17}$. ΔN, the difference between level 2 and level 3, is 3.5830×10^{18}. The Q_m given by Eq. 3.4-2 is 11.77, a factor of 1.88 higher than the Eq. 3.4-1 approximation. Use of the approximation is not acceptable for the higher frequency and lower temperature Q_m calculations.

The gain of a maser depends upon Q_m and upon the interaction time between the RF magnetic field and the spin system. The interaction time in a cavity maser is dependent on Q_1, the loaded *Q* of the cavity. The cavity maser electronic gain equation in decibels is

$$G_e^{dB} = 10 \cdot \log\left[\frac{(Q_1 + Q_m)}{(Q_1 - Q_m)}\right]^2 \tag{3.4-4}$$

The interaction time in a TWM is dependent upon the TWM's electrical length, the slowing factor (*S*) multiplied by the physical length in wavelengths (*N*). The TWM electronic gain equation in decibels is

$$G_e{}^{dB} = \frac{(27.3) \cdot S \cdot N}{Q_m} \tag{3.4-5}$$

These equations are simplified but accurate forms, derived from those found in [6, pp. 268 and 309]. Ruby masers developed at JPL from 1959 through 1992 were based on the material described above. These designs were analyzed by using performance measurement data of the amplifying structures.

Future waveguide-cavity maser designs and TWMs using waveguide resonators as slow-wave structures can be analyzed using computer programs. Various 32-GHz ruby maser designs have been created and analyzed using a combination of commercial design software and a specialized JPL-developed program based on a waveguide mode-matching algorithm. The new analysis of maser designs will be described in a later part of this chapter.

3.5 Ruby Maser Noise Temperatures

A distinct advantage of the ruby maser is its low effective input noise temperature (T_{ampl}). It is also an advantage that the maser noise temperature can be calculated accurately and reliably from the maser gain-and-loss characteristics. The maser net gain, the structure loss, the ruby "pump off" spin-system loss, and the thermodynamic or bath temperature of the maser (T_{b}) are needed for the noise temperature calculation.

The equation used for an accurate calculation of a ruby maser's equivalent input noise does not require that hf/kT be much less than one. It is accurate at all frequencies and temperatures, and it includes the quantum noise contribution. The maser's noise temperature is predicted with calculations broken into two parts. The first part accounts for the noise temperature of the ruby spin system. The second part accounts for noise contributed by the dissipative losses in the slow-wave structure of a TWM, RWM, or in the resonators of a cavity maser. Noise contributions from dissipative losses in components preceding the maser must be accounted for separately.

Siegman has described and discussed noise, in masers and in general [6, p. 398], and Siegman derives the noise power from a maser to be

$$P_{n(\text{ampl})} = (G-1)\cdot\left[\frac{\alpha_m}{\alpha_m-\alpha_0}P_n(-\alpha_m,-T_m)+\frac{\alpha_o}{\alpha_m-\alpha_o}P_n(\alpha_o,T_o)\right] \qquad (3.5\text{-}1)$$

where Siegman's symbols, α_m and α_o, are the electronic gain and loss coefficients per unit length, $(\alpha_m-\alpha_o)$ is the net gain coefficient per unit length, and T_s, the spin temperature, equals $-T_m$. This expression is valid for a traveling-wave maser (TWM), a reflected-wave maser (RWM), and the reflection-type cavity maser.

Numerically, the gain and loss coefficient ratios can be replaced by ratios of the maser's electronic gain $G_e^{(dB)}$, net gain $G^{(dB)}$, and loss $L_o^{(dB)}$ in decibels. Therefore, $\alpha_m/(\alpha_m-\alpha_o)$ equals $G_e^{(dB)}/G^{(dB)}$ and $\alpha_o/(\alpha_m-\alpha_o)$ equals $L_o^{(dB)}/G^{(dB)}$, where the electronic gain is provided by the inverted ruby spin system and the loss is the signal attenuation due to dissipation. The dissipation is caused by the resistance of the copper or other metals used in the structure, by dielectric material loss, and by ferrite or garnet isolator forward loss in the case of a TWM. This loss term, $L_o^{(dB)}$, does not include the spin-system signal absorption that occurs when the maser is not pumped. The net gain in decibels is the electronic gain in decibels minus the loss in decibels.

Using the measured gain and loss values in decibels, and replacing $P_n(T)$ with the Planck radiation law

$$P_n(T) = \frac{h\,fB}{e^{\frac{h\,f}{k\,T}}-1} \qquad (3.5\text{-}2)$$

The equation for the noise power from the maser becomes

$$P_{n(\text{ampl})} = (G-1)\left\{\left(\frac{G_e{}^{dB}}{G^{dB}}\right)\left(\frac{\text{h}\,fB}{1-e^{\frac{-\text{h}\,f}{\text{k}T_m}}}\right)+\left(\frac{L_o{}^{dB}}{G^{dB}}\right)\left(\frac{\text{h}\,fB}{e^{\frac{\text{h}\,f}{\text{k}T_o}}-1}\right)\right\} \tag{3.5-3}$$

and the noise temperature of the maser becomes

$$T_{\text{ampl}} = \left(\frac{G-1}{G}\right)\left(\frac{\text{h}\,f}{\text{k}}\right)\left\{\left(\frac{G_e{}^{dB}}{G^{dB}}\right)\left(\frac{1}{1-e^{\frac{-\text{h}\,f}{\text{k}T_m}}}\right)+\left(\frac{L_o{}^{dB}}{G^{dB}}\right)\left(\frac{1}{e^{\frac{\text{h}\,f}{\text{k}T_o}}-1}\right)\right\} \tag{3.5-4}$$

The spin temperature is determined by the ratio of the spin population densities in the two levels associated with the signal transition.

$$r = \frac{n_i}{n_j} = e^{\frac{-\text{h}\,f}{\text{k}T_s}} = e^{\frac{\text{h}\,f}{\text{k}T_m}} \tag{3.5-5}$$

The ratio *r* is substituted in Eq. (3.5-4), resulting in the simplified form

$$T_{\text{ampl}} = \left(\frac{G-1}{G}\right)\left(\frac{\text{h}\,f}{\text{k}}\right)\left\{\left(\frac{G_e{}^{dB}}{G^{dB}}\right)\left(\frac{r}{r-1}\right)+\left(\frac{L_o{}^{dB}}{G^{dB}}\right)\left(\frac{1}{e^{\frac{\text{h}\,f}{\text{k}T_o}}-1}\right)\right\} \tag{3.5-6}$$

"Pump saturation" is a requirement meaning the pump power is sufficient to equalize the spins in the energy levels spaced properly for pump excitation. Verification of this pump-saturated condition is determined by increasing the pump power until no further increase in maser gain is observed. The pump-saturated inverted spin population density ratio between levels *i* and *j*, denoted by $r = n_i / n_j$, is determined by the difference between the thermal equilibrium level spin densities and the inversion ratio *I*.

$$I = \frac{n_i - n_j}{N_j - N_i} = \frac{G_e{}^{dB}}{L_r{}^{dB}} \tag{3.5-7}$$

N_i is the spin population of level *i* when the spin system is in thermal equilibrium, and n_i is the spin population in level *i* when the ruby spin system is saturated with pump power. The inversion ratio is numerically equal to the ratio of the electronic gain in decibels, with the microwave pump source on, to the ruby absorption in decibels, $L_r^{(dB)}$, with the microwave pump source off.

Depending on the pumping scheme, the expression for r is different. For the three-level system used at S-band, at the 90-deg orientation, the signal transition is between levels 1 and 2, and the pump transition is between levels 1 and 3. The 4th level is not involved, and the number of spins in it is unaffected by the pumping. Pumping equalizes the number of spins in levels 1 and 3, and two equations for the populations in each level are:

$$n_2 - n_1 = I(N_1 - N_2) \tag{3.5-8}$$

and

$$n_2 + 2n_1 = N \tag{3.5-9}$$

where N is the total number of spins in levels 1, 2, and 3; and

$$N = N_1 + N_2 + N_3 = n_1 + n_2 + n_3$$

Multiplying Eq. (3.5-8) by 2 and adding the resulting product to Eq. (3.5-9) results in

$$3n_2 = N + 2I(N_1 - N_2) \tag{3.5-10}$$

Subtracting Eq. (3.5-8) from Eq. (3.5-9) results in

$$3n_1 = N - I(N_1 - N_2) \tag{3.5-11}$$

Dividing Eq. (3.5-10) by Eq. (3.5-11) results in

$$r_s = \frac{1 + 2I(N_{1'} - N_{2'})}{1 - I(N_{1'} - N_{2'})} \tag{3.5-12}$$

where $N_{i'} = N_i / N$

A four-level push-push pumping scheme is used at X-band and Ku-band, and it may also be used at S-band. The signal transition is between levels 1 and 2, and the pump transitions are between levels 1 and 3 and also between levels 3 and 4. Calculating the spin densities in the four levels, using the knowledge that levels 1, 3, and 4 are equalized by pumping, and using the measured inversion ratio I, the ratio of spins in level 2 divided by level 1 is

$$r_x = \frac{1 + 3I(N_{1'} - N_{2'})}{1 - I(N_{1'} - N_{2'})} \tag{3.5-13}$$

where $N_{i'} = N_i / N$ and N is the total number of spins in levels 1, 2, 3, and 4.

A four-level push-pull pumping scheme is used with JPL masers at K-band and Ka-band. The signal transition is between levels 2 and 3, and the pump transitions are between levels 1 and 3 and also between levels 2 and 4. The 54.7-deg ruby orientation produces symmetrical energy levels, so that the 1–3 transition is equal to the 2–4 transition. Calculating the spin densities in the four levels is similar to the processes above. Using the knowledge that the spin density in level 1 equals the spin density in level 3, and that the spin density in level 2 equals the spin density in level 4, and the using the measured inversion ratio *I*, the ratio of spins in level 3 divided by level 2 is

$$r_k = \frac{1 + 2I(N_{1'} - N_{2'})}{1 - 2I(N_{1'} - N_{2'})} \tag{3.5-14}$$

where $N_{i'} = N_i / N$

In contrast with the noise temperature calculations described above, a very simple equation can be used to calculate the approximate noise temperature of a maser (T_{maprx}) when $\text{h}f / \text{k}T$ is much less than one and when the maser gain is very high [5].

$$(T_{\text{maprx}}) = T_b \frac{L_t^{(dB)}}{G^{(dB)}} \tag{3.5-15}$$

where $L_t^{(dB)}$ is the forward loss through the maser structure in decibels with the pump turned off. This loss includes all dissipative losses, such as resistive losses in copper, forward isolator losses, dielectric losses and the ruby (spin-system) signal absorption. $G^{(dB)}$ is the net gain of the maser in decibels. T_b is the thermodynamic temperature or bath temperature of the ruby. A comparison of the results is shown in Table 3-3.

Table 3-3. T_{maprx} values compared with accurate T_{ampl} calculation results.

Parameter	Value			
Frequency (GHz)	2.295		8.430	33.7
Bath temperature (T_b) (K)	4.5	1.6	4.5	1.5
T_{maprx} (K)	1.61	0.89	2.15	0.83
T_{ampl} (K)	1.64	1.02	2.23	2.33
Difference (K)	–0.03	–0.13	–0.08	–1.50

Table 3-3 shows reasonable T_{maprx} values for S-band masers at 2295 MHz and X-band masers at 8430 MHz operating at a bath temperature of 4.5 K. The value of hf/kT is 0.0245 at 2295 MHz and 4.5 K, and 0.0899 at 8430 MHz and 4.5 K. At 8430 MHz and a bath temperature of 1.6 K, the value of hf/kT is 0.2529, and the error of the T_{maprx} calculation is about <15 percent. It seems best to use the more accurate noise temperature calculation when hf/kT is greater than 0.1. Maser performance values used to calculate the maser noise temperatures are shown in Table 3-4.

Variations of maser noise temperature caused by changes in loss, inversion ratio, and bath temperature are quantified to help determine the accuracy of the maser noise temperature. For example, the TWM at 2295 MHz in Table 3-3 is based on a slow-wave structure forward loss of 5 dB. An increase of 1 dB in the structure forward loss value causes a noise temperature increase of 0.12 K. An inversion ratio reduction from 4.5 to 4.0 causes a noise temperature increase of 0.14 K. An increase in the bath temperature from 4.5 K to 4.7 K causes a gain reduction of 2 dB and a noise temperature increase of 0.10 K. Maser performance characteristics at 8430 MHz and 33.7 GHz can be measured to accuracies that are little different than those at 2295 MHz. For example, at 33.7 GHz and a bath temperature of 1.5 K, a bath temperature increase to 1.7 K increases the maser noise temperature by less than 0.1 K. Similar percentage changes of loss and inversion ratio cause maser noise temperature changes of less than 0.1 K. Based on these sensitivity values and our ability to measure maser performance gain and loss characteristics to a fraction of a dB, and the bath temperature to better than 0.1 K, all calculated maser noise temperatures are expected to be accurate to within ± 0.1 K.

These T_{ampl} maser noise temperature values are for the input to the ruby maser at the bath temperature. In the case of a cavity maser, the noise contribution of the circulator preceding the cavity amplifier must be added. In all cases, any loss preceding the maser adds noise to the maser and the

Table 3-4. Maser performance values for noise temperature calculations.

Parameter	Value			
Signal frequency (GHz)	2.295	8.430		33.7
Bath temperature (T_b) (K)	4.5	4.5	1.6	1.5
Net gain (dB)	45.0	45.0	34.0	27.0
Electronic gain (dB)	50.0	49.0	39.0	28.0
Structure loss (dB)	5.0	4.0	5.0	1.0
Inversion ratio	4.5	2.8	2.8	2.0

appropriate correction must be used to determine the effective input temperature at the ambient interface.

The input transmission line from the maser to the ambient interface and the vacuum seal add about 0.5 K ±0.1 K for the Block IV S-band maser described. The effective input noise temperature (T_{m}) of the S-band Block IV maser is 2.1 K ±0.2 K at the ambient interface.

The waveguide input system from the maser to the ambient interface and the vacuum window add about 1.0 K ±0.4 K for the Block II X-band maser described. The Block II X-band maser operates in a closed cycle refrigerator at a bath temperature of 4.5 K. The effective input noise temperature of the maser is 3.5 K ±0.5 K at the ambient interface. The X-band maser cooled to 1.6 K has an effective input noise temperature of 1.8 K ±0.4 K.

The 33.7-GHz cavity maser operates in super-fluid helium at a bath temperature of 1.5 K. The loss of a circulator and isolator preceding the first stage cavity, cooled waveguide, and a partially cooled feed horn with a vacuum window at the ambient interface add about 2.7 ±1 K. The effective input noise temperature of this maser is 5.0 K ±1 K at the ambient interface.

Measurement of a maser's effective input noise temperature using hot and cold loads at 300 K and 80 K is often done in the laboratory at JPL and in the DSN. Using the maser's calculated effective input noise temperatures above (T_m without the tolerances shown), and using the Planck Radiation Law correction for the noise power from the loads, the amplifier output power ratio (Y-factor) obtained while switching from the hot load to the cold load can be calculated. Using this calculated power ratio and the Rayleigh-Jeans approximation for hypothetical hot and cold load measurements gives slightly different maser effective input noise temperatures (T_{m2}). The results are shown in Table 3-5.

The use of T_m for the maser's effective input noise temperature here is the same as the use of T_{lna} for the low-noise amplifier effective input noise

Table 3-5. T_m calculated results compared with hypothetical measurement results (T_{m2}) from the use of the Rayleigh–Jeans approximation with reference loads at 300 K and 80 K.

Parameter	Value			
Frequency (GHz)	2.295	8.430		33.7
T_b (K)	4.5	1.6	4.5	1.5
T_m (K)	2.1	1.8	3.5	5.0
T_{m2} (K)	2.045	1.598	3.298	4.195
Difference (K)	0.055	0.202	0.202	0.805
h*f*/2k (K)	0.055	0.202	0.202	0.809

temperature in other chapters of this book. Table 3-5 shows the differences in the effective input noise temperature of masers caused by the differences in the reference load noise powers that result from the use of the Rayleigh–Jeans approximation. These differences are very close to one-half of the quantum noise ($hf/2k$) for the cases analyzed. A more detailed explanation of this result was published previously [8,9]. System operating noise temperature measurements in the DSN currently use the Rayleigh-Jeans approximation.

3.6 Ruby Masers as Noise Temperature Standards

The DSN ruby masers used as pre-amplifiers to achieve the lowest practical receiving system noise temperatures are also used as noise standards. The maser's effective input noise temperature (T_m) determines the receiver's effective input noise temperature (T_e) and enables the accurate measurement of the total receiving system's operating noise temperature (T_{op}). T_{op} is the sum of T_e and the antenna output temperature (T_i). T_{op} here is defined at the ambient input terminal of the maser, which is the reference 2 location defined in Chapter 2. In this case, T_i includes the sky brightness temperature, antenna pickup from ambient surroundings, noise contributed by reflector losses, and noise contributed by feed system loss when the feed system components are at ambient temperature. Use of masers as noise standards eliminates the need for cryogenically cooled reference terminations in DSN receiving systems.

DSN receiving systems use a waveguide switch and a room temperature load, or an ambient temperature absorber (aperture load) that can be positioned in front of the antenna feed-horn. The aperture load is used to terminate the receiver with a resistive source of known (ambient) temperature. The power ratio measured when the receiver's input is switched from the ambient load to the antenna is used to determine T_{op}.

DSN ruby masers at 2295 MHz, 8430 MHz, and 33.70 GHz achieved effective input noise temperatures of 2.1 K ±0.2 K, 1.8 K ±0.5 K, 3.5 K ±0.5 K, and 5.0 K ±1.0 K respectively, as explained in the previous paragraphs. The measured values agreed with the calculated maser effective input noise temperatures (T_m) at the maser's ambient interface.

The receiver's effective input noise temperature (T_e) is the sum of the maser noise temperature (T_m) and the follow-up receiver noise contribution. High DSN maser gain (typically 45 dB) reduces the follow-up receiver noise contribution to a value that can be measured in two different ways. The follow-up receiver noise temperature can be measured using hot and cold loads. The measured receiver noise temperature is then divided by the maser gain to determine the receiver's contribution to T_{op}. For example, when the noise

temperature of the receiver following the maser is 1000 K and the maser gain is 45 dB (31,623), the follow-up receiver contribution (T_f) to T_a is 1000/31623 = 0.0316 K.

Turning the maser pump source off and on and measuring the resulting receiver power ratio is another method to determine (T_f). This technique, suggested by Dr. R. W. DeGrasse in 1962[1], has been used since in the DSN. In this case, the maser with a 2.1-K noise temperature is connected to an ambient termination near 290 K and receiver output power ratio, Y_{pump}, is measured while turning the maser pump source off and on.

Without the knowledge of the follow-up receiver noise temperature, as used in the first example,

$$\frac{T_{\text{amb}} + T_a + T_f}{T_f} = Y_{\text{pump}} \tag{3.6-1}$$

and

$$T_f = \frac{T_{\text{amb}} + T_a}{Y_{\text{pump}} - 1} \tag{3.6-2}$$

Substituting the known values for the ambient load (290 K for example) and the maser we find

$$T_f = \frac{290\ \text{K} + 2.1\ \text{K}}{Y_{\text{pump}} - 1} \tag{3.6-3}$$

A large value of Y_{pump} is observed when the maser gain is 45 dB. The 1000-K follow-up receiver temperature mentioned above results in a 39.66-dB Y_{pump} measurement. A 10,000-K follow-up receiver temperature would result in a 29.66-dB Y_{pump} measurement, indicating a 0.316-K follow-up receiver contribution. A phone call to a receiver repair person would be in order following such a receiver noise temperature measurement.

A small error in T_f occurs when using the pump on–off method if the maser's pump-off loss is low, and a low-noise follow-up amplifier is used with a maser having modest gain. This error occurs when the noise from the ambient load, attenuated by the maser's pump-off loss, is a significant fraction of the follow-up amplifier noise temperature. Performance values for the 33.68-GHz

[1] Personal communication from Dr. R. W. DeGrasse to R. Clauss in 1962.

dual cavity maser are used here for example. The pump-off loss of 17 dB (14 dB ruby absorption and 3 dB microwave component loss) allows 6 K from a 300-K ambient load to reach the follow-up amplifier. The cooled high electron mobility transistor (HEMT) follow-up amplifier had an effective input noise temperature of 40 K. At 25-dB maser gain, the follow-up noise temperature was 0.1265 K. Using the pump on/off technique results in a follow-up calculation of 0.1455 K which is high by 0.019 K.

When the maser in the examples above is switched from the ambient load to the antenna, the measured power ratio $(Y_{\text{amb-ant}})$ is used to determine T_{op}.

$$T_{\text{op}} = \frac{T_{\text{amb}} + T_m + T_f}{Y_{\text{amb-ant}}} \tag{3.6-4}$$

For example, when ($Y_{\text{amb-ant}}$ is equal to 25.12 (14.00 dB), T_{op} = 11.624 K. This S-band example is used because it is similar to the results achieved with the DSN's S-band receiving system on the 70-m antenna in Australia (DSS-43) used to support the Galileo Mission during recent years. This S-band maser was originally developed to support the Mariner-10 Mercury encounters in 1974 [10]. T_{op} measurements at X-band and Ka-band in the DSN use the same techniques described above.

The accuracy of the ruby maser's effective input noise temperature affects the accuracy of the system operating noise temperature measurement when the maser is used as a noise standard. The S-band example can be used to show that a 0.2-K error in maser noise temperature results in a 0.008-K error in T_{op}. The error is very small because the $(Y_{\text{amb-ant}})$ ratio is large. T_{op} values measured with the antenna at the zenith, looking through one atmosphere in clear dry weather, range from the S-band low value to typical values of near 20 K at X-band and 30 K for the 33.70-GHz maser system used at DSS-13. The T_{op} error caused by a T_m error is proportional to T_{op}. For example, a 1-K error in T_m causes a 0.07-K error in T_{op} when T_{op} is 21 K, a 0.1-K error when T_{op} is 30 K, and a 0.2-K error when T_{op} is 60 K.

Directional couplers are used in a DSN receiving system to inject signals before and after the maser preamplifier to measure the maser gain. The directional coupler between the antenna feed and the maser is also used to inject a small amount of noise from a noise source (gas tube or noise diode). An advantage of using a small amount of injected noise, that can be turned on and off, is to monitor T_{op} without disconnecting the receiver from the antenna. The injected noise pulse becomes a secondary measurement standard; the noise

pulse excess temperature is determined by comparison with the total system noise power when the maser is connected to the ambient load.

Another important advantage occurs when injecting a signal, or a small amount of noise, while the receiver is alternately connected to the antenna, and the ambient temperature termination. This technique enables the detection of receiver gain changes that might occur when the receiver is switched from the antenna to the ambient termination. Measurement of any receiver gain change that occurs when switching between the antenna and the ambient termination can be used to correct the error that results from the receiver gain change.

Loads or terminations at different temperatures, often at cryogenic and ambient temperatures, can be used to measure receiver noise temperatures. The effective noise temperature of loads at temperatures other than ambient depend upon accurate knowledge of the dissipative surface of the load, and the temperature gradient and loss of the transmission line used to thermally isolate the load from the switch between the receiver and the load. Errors in the effective temperature of cryogenically cooled loads can be caused by moisture condensing upon portions of the interconnecting transmission lines and windows (or gas barriers) required to separate the cryogenic system from the ambient environment.

The maser noise temperature, based on calculations and other performance measurements, is known to the accuracy described above. The input waveguides and transmission lines of the TWMs in CCRs are in a vacuum environment, eliminating the dangers of moisture getting into the lines. The maser's gain affects the maser's noise temperature and is easily measured. A maser gain reduction of 3 dB (out of 45 dB) occurs when the cryogenic temperature of the maser increases from 4.5 K to 4.8 K. The resulting noise temperature increase is 0.165 K for the S-band Block IV TWM and 0.33 K for the X-band Block II TWM. The maser gain is specified to be 45 dB ±1 dB, and noise temperature fluctuations will be accordingly less than 0.06 K at S-band and 0.11 K at X-band.

The effective noise temperature of an ambient load, combined with the use of the noise temperature of a low-noise amplifier with an accurately known noise temperature, eliminates the need for cryogenically cooled reference terminations in deep-space receiving systems. This measurement technique with ruby masers has been used for forty years at the operational DSN frequencies. The values of the total system operating noise temperatures needed for telemetry link evaluations can be measured to an absolute accuracy of better than 1 percent by using the maser as a noise standard.

3.7 Immunity from Radio Frequency Interference (RFI)

Ruby masers use cavities or a slow-wave structure to increase the interaction time between the ruby spin system and the microwave signal. The

cavity, or slow-wave structure, behaves like a filter. The filter properties of the microwave structure provide out-of-band rejection to unwanted signals (RFI). Unwanted, interfering signals within the maser structure bandwidth do not cause measurable inter-modulation products. The measured conversion loss exceeds 100 dB when a ruby maser is subjected to two unwanted input signals within the maser's amplifying bandwidth, at levels as great as –80 dBm. The maser is not a good mixer. In-band signals sufficiently large to cause an amplified maser continuous output level of greater than 0.3 μW reduce the spin population difference associated with the signal transition and reduce the maser gain.

3.8 Early DSN Cavity Masers

Cavity masers mentioned earlier in this chapter were used on DSN antennas at 960 MHz, experimentally in 1960, and later to receive signals from spacecraft going to Venus and to the moon [1]. Cavity masers at 2388 MHz were used to receive radar echoes from Venus and Mars.

The 1961 Venus radar experiment used a 13-kilowatt (kW) transmitter on a 26-m antenna at the Echo Site, and a single-cavity 2388-MHz ruby maser radar receiver preamplifier at the Pioneer Site. The radar receiver achieved a system operating noise temperature of 64 K. William Corliss, in *A History of the Deep Space Network* [1] wrote:

> "… This radar was operated in a two-way, phase coherent mode. Over 200 hours of good data were obtained while Venus was between 50 and 75 million miles from earth.
>
> A scientific result that was also of immense practical importance was the radio determination of the Astronomical Unit (A.U.) as 149, 598, 500 ±500 km, an improvement in accuracy of nearly two orders of magnitude. If the old optical value of the A.U. had been used in the Mariner-2 trajectory computations, its flyby of Venus might have been at a much greater distance with a resultant loss of scientific data."

Experience and information obtained through the use of the cavity masers on DSN antennas at Goldstone have been of great value to the designers and builders of DSN ruby masers. The most important lesson learned by those developing these masers (which were new types of equipment to many and destined for use in the field on large, fully steerable antennas in an operational environment) was the following.

New types of equipment, such as these ruby masers going into the field, should be accompanied by the developers. The developers of new masers should operate, service, and maintain the new equipment in the operational environment for at least several weeks. A quick, one-day, or one-week check-out is not adequate.

Additional lessons learned include the following:

1) Laboratory testing of masers planned for use in the DSN is not sufficient until the field environment is understood well enough to develop all of the needed tests.
2) Support personnel in the field operating, servicing, and maintaining masers will often be blamed for equipment failures beyond their control.
3) Support personnel who will operate, service, or maintain masers should be given appropriate training and documentation that includes installation, operations, and maintenance procedures.
4) Maser developers must understand the electrical and mechanical interfaces to the adjacent subsystems and design the interfaces to withstand mechanical and electrical strain and stress. An example of the needed interface understanding follows. A massive S-band waveguide section from the antenna feed system was attached to the type N connector on the circulator at the input to the maser. Antenna motion caused movement that broke the circulator. Circulators were new and expensive devices in February 1961, and we did not have a spare. The circulator was repaired on site by two very nervous technicians.
5) Maser support personnel working in the DSN should understand the entire receiving system sufficiently well to identify failures that occur in other subsystems. Otherwise any receiving system failure will be identified as a maser failure by the other subsystem engineers.
6) Instrumentation to monitor the cryogenic system's condition and a simple receiver used to measure the maser's performance were essential.
7) The effectiveness of vacuum insulation in a liquid helium dewar system, in a liquid helium transfer line, or in the vacuum housing of a closed-cycle helium refrigerator, is destroyed by the introduction of a very small amount of helium gas. Helium diffusion through rubber o-ring seals, vacuum windows in waveguides and connectors that are made from materials that are not impervious to helium allows helium gas to enter the vacuum jacket.
8) There is no substitute for long-term experience in the field environment. Systems should be field-tested on antennas having an environment as close as possible to the operational environment planned for mission support. Planetary radar tasks provided ideal field experience with systems planned for lunar and interplanetary mission support.
9) Adding a few "improvements" will sometimes disable a system that has worked well previously.
10) The best engineers sometimes make mistakes. This list could be much longer.

A dual-cavity maser at 2388 MHz was used on the 26-m antenna at DSS-13, the "Venus" site in the fall of 1962 for planetary radar to study Venus,

and in 1963 to receive radar echoes from Mars. The environment of an elevation-over-azimuth-drive (Az-El) with a cassegrain feed system was preferred over the prime-focal-point location of the 26-m polar mount antennas by those designing, building, and servicing ruby masers. Liquid helium and liquid nitrogen transfers were made from the antenna's main reflector surface through the wall of the cassegranian feed cone. The thrill of "high altitude" liquid helium transfers from the cherry-picker-bucket being buffeted by high winds was gone and not missed. The antenna elevation motion was from 10 deg above the horizon to the zenith (90-deg elevation). The maser package was mounted at an angle such that the dewar containing the maser and cryogens did not tilt more than 50 deg from vertical, thereby avoiding liquid cryogen spills. A cross-sectional view of one of the two identical units is shown in Fig. 3-4. The first circulator was an S-band waveguide configuration, providing a waveguide interface to the antenna feed system.

The noise temperature of the dual-cavity maser was determined by the loss of the ambient temperature circulator, the loss of a waveguide-to-coaxial-line transition, the loss of the 7/8-inch (~2-cm) diameter coaxial line transition, and the maser in the 4.2-K bath. These losses contributed about 16 K, bringing the maser's effective input noise temperature to 18 K ±2 K. A 35-K total system noise temperature was achieved for the radar receiving system, a significant improvement over the 64-K system at the Pioneer site.

3.9 Comb-Type Traveling-Wave Masers

Bell Telephone Laboratories (BTL) headquartered at Murray Hill, New Jersey with greatest concentration of facilities in northern New Jersey and Airborne Instruments Laboratories (AIL) in the Long Island area had demonstrated and published the characteristics of S-band traveling-wave masers (TWMs) in 1959 and 1960 [11,12]. The TWMs used a comb-type slow-wave-structure (SWS), ruby, and polycrystalline yttrium-iron-garnet (YIG) resonance isolators. The SWS is like a resonant comb-type band-pass filter. Incoming microwave signals to be amplified were coupled into the SWS from a coaxial line and traveled through the SWS at a speed as low as 1/100 the speed of light (the group velocity). The slowing-factor of the SWS is the reciprocal of group velocity divided by the speed of light. Ruby bars were located on both sides of the comb, and the spin system in the ruby provided the signal-frequency amplification. The signal's interaction with the spin system is proportional to the slowing factor. Resonance isolators were located in regions of circular polarization on one side of the comb. These isolators provided high attenuation in the reverse direction to enable stable, regeneration-free amplification of microwave signals traveling in the forward direction.

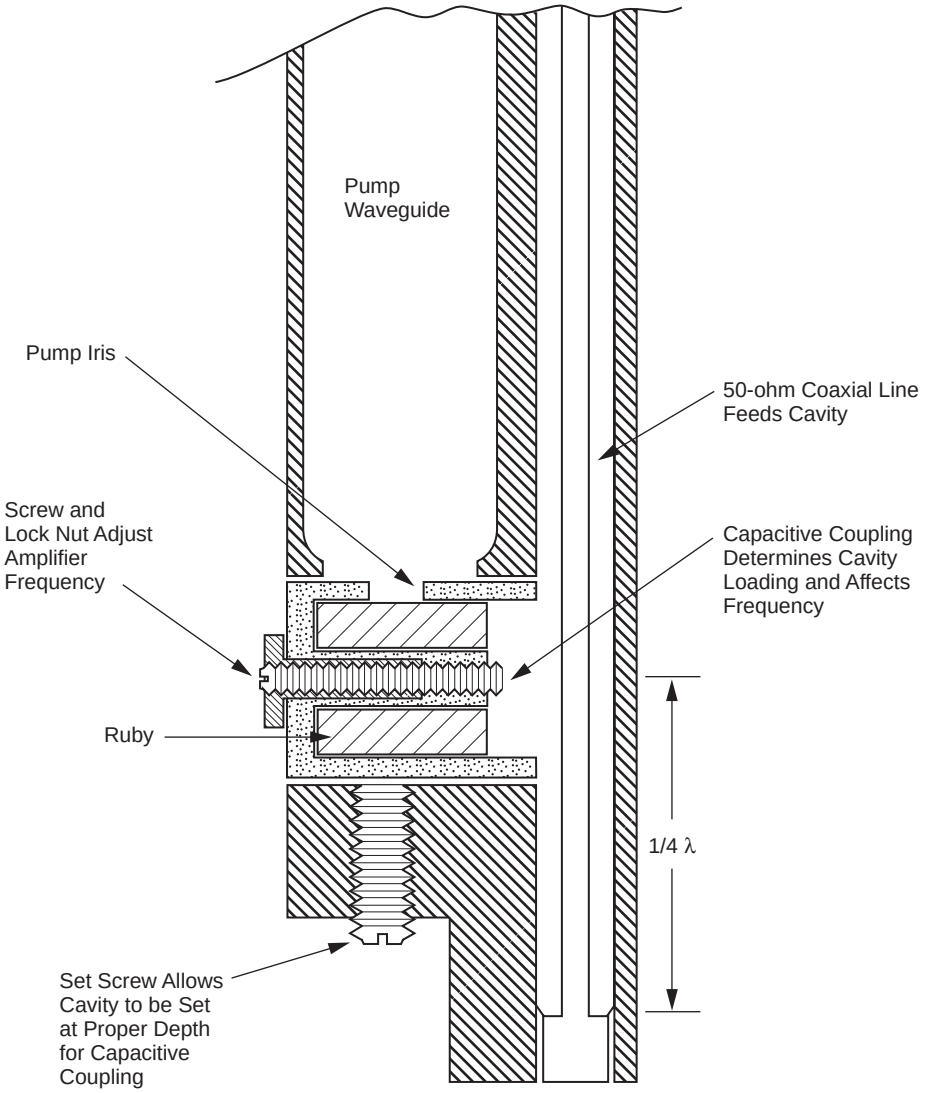

Fig. 3-4. Cross-section of one cavity of the two-cavity maser.

Dr. Walter Higa's group at JPL had concentrated on the development of the cavity masers needed for planetary radar and early mission support prior to 1963. The need to support future missions requiring more bandwidth than the cavity masers were able to provide resulted in the decision to purchase traveling-wave masers from those who were TWM experts. Dr. Robert W. DeGrasse had moved from BTL to the Microwave Electronics Corporation (MEC), providing another commercial source for TWMs. MEC developed a TWM for JPL in 1962. The TWM covered the S-band 2290-MHz to 2300-MHz

allocation for deep-space-to-Earth communications, and it was tunable to the 2388-MHz planetary radar frequency. Signal input transmission line loss and instabilities, and a fragile vacuum seal in that transmission line, prevented use of the MEC TWM in the DSN.

JPL purchased six TWMs for the DSN from AIL in 1964. Six closed-cycle refrigerators (CCRs) were purchased from Arthur D. Little (ADL) to provide 4.5-K cryogenic cooling for the TWMs. The maser group at JPL developed low-loss transmission lines, produced packages that supported a rugged S-band waveguide input interface, and integrated the TWMs and CCRs into antenna-mountable units with the power supplies, controls, instrumentation, and support equipment needed for the complete maser subsystems. The TWM/CCR subsystems included antenna cabling and helium gas lines connecting the helium compressor located near the antenna base, to the TWM/CCR package located in the cassegrain cone of the 26-m polar-mount antennas. Figure 3-5 is a photograph of the Block I S-band TWM package, and Fig. 3-6 is a block diagram of the Block I S-band subsystem.

Operations of these Block I TWM subsystems at DSS-11 (Pioneer Site at Goldstone, CA), DSS-12 (Echo Site at Goldstone, CA), DSS-41 (Woomera, Australia), DSS-42 (near Canberra, Australia), and DSS-51 (near Johannesburg, South Africa) supported the successful Mariner IV Mars encounter in July 1965. The play-back sequence of our first close-up photographs of the Martian surface returned one picture every eight hours. The data rate was 8.33 bits per second. These five TWM/CCR subsystems all performed without failure during the two-month picture playback period. A sixth Block I TWM subsystem was installed at DSS-61 in Robledo (near Madrid), Spain.

Eight more TWM/CCR systems using AIL TWMs and ADL CCRs were added to the DSN between 1965 and 1968. The eight new systems were identified as Block II S-band TWMs. The S-band Block II TWMs were modified to support the planned Manned-Space-Flight-Network (MSFN) frequencies (2270 MHz to 2290 MHz) as well as the Deep-Space-to-Earth frequency allocation (2290 MHz to 2300 MHz). Future missions with additional requirements, and the limited performance and life-times of the ADL CCRs showed the need for further TWM and CCR development work.

The business environment of that time affected JPL's and NASA's TWM and CCR development approach. Future users of TWMs in the commercial sector seemed limited. Earth-orbiting satellite communications networks did not need very low noise receiving systems in the many Earth-based (ground) installations. Earth-orbiting satellites, sending information to ground stations, could put more transmitter power on the satellite and eliminate the need for a multitude of cryogenically-cooled receivers on the ground. Ambient temperature preamplifiers for the ground-based receivers would have adequate sensitivity, and they would still cost less, be less expensive to maintain, and be more reliable than cooled-receiver preamplifiers.

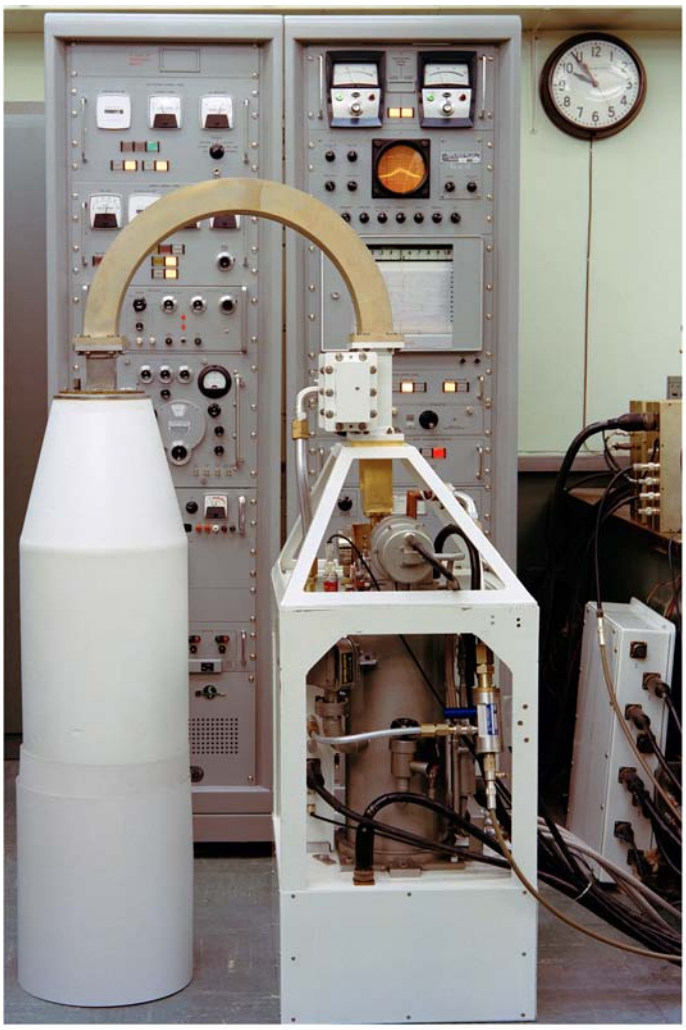

Fig. 3-5. Block I S-band TWM package during laboratory evaluation.

Most of the organizations and specialized personnel that had developed maser technology seemed anxious to move on to the optical spectrum. Light amplification by stimulated emission of radiation (laser) development work attracted many of the specialists who had worked on maser development. Those who continued developing masers after 1965 were, for the most part, concerned with deep-space communications or radio astronomy.

The success and experience with the Block I S-band masers during the Mariner IV mission to Mars showed the potential for future use of TWMs in the DSN. TWM/CCR subsystems with increased performance and reliability would

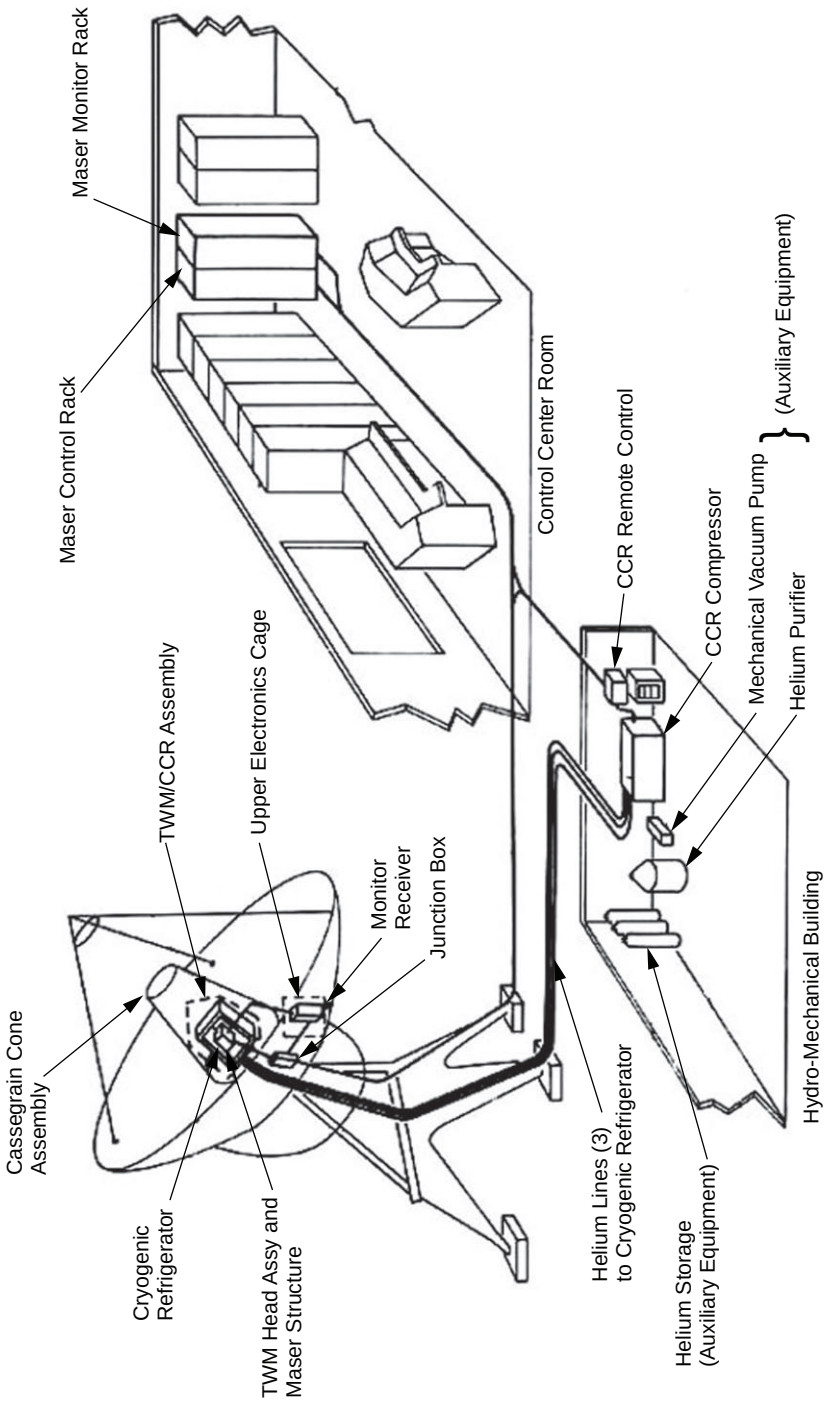

Fig. 3-6. Block I S-band subsystem block diagram.

be needed in the DSN. Future missions would utilize near-real-time video transmission from deep space to Earth. Data rates as high as 117,000 bits per second (kbps) would be used from a distance of about 5 A.U.

Dr. Walter Higa's and Ervin Wiebe's work on CCR development was aided by Professor William Gifford, a co-inventor of the Gifford McMahon (GM) cycle. Their work resulted in a JPL design for a CCR with a simplified cool-down procedure, a quicker cool-down time, and a mean time between failures (MTBF) that was increased from the previous 1500 hours to 3000 hours. Beginning in 1966, the first of these new CCRs was operated on Goldstone's 64-m antenna at DSS-14 for 20,000 hours without maintenance or failure. More about these CCRs will follow in the Cryogenic Refrigeration Systems chapter.

The development of new TWMs with significant performance improvement goals began in 1965. This work took advantage of the previously learned lessons and the knowledge obtained from the material published so generously by the TWM experts at BTL and AIL. New technology developed by the JPL maser team resulted in several patents [39–53]. S-band TWMs tunable from 2275 MHz to 2415 MHz were developed for use on the 26-m antenna at DSS-13 and on the 64-m antenna at DSS-14. S-band Block III and Block IV TWMs, covering 2265 MHz to 2305 MHz, X-band TWMs operating across a tuning range extending from 7600 MHz to 8900 MHz, and a Ku-band TWM tunable from 14.3 GHz to 16.3 GHz were also developed between 1965 and 1973.

Goals of the TWM development work at JPL were to maximize the TWM gain and bandwidth while minimizing the noise temperatures. Comb-type slow-wave structure loss (called forward loss) reduces the TWM gain and raises the noise temperature. High reverse loss, accomplished by resonance isolators in the slow-wave structure is needed for stable, non-regenerative amplification.

Initial attempts to produce copper comb-type slow-wave structures without joints in the regions of high-intensity RF magnetic fields were unsuccessful. The use of milling machines with various types of cutters (including saws and end-mills) did not yield sufficient precision. Experienced and knowledgeable machinists in the JPL machine shop developed techniques using a shaper and extremely hard carbide-alloy cutting tools to cut groves into copper with the needed precision. Electric discharge machining (EDM) was used to create a comb structure from the ribs of copper left between the grooves.

The first of a series of copper TWM comb-structures produced with this technique is shown in Fig. 3-7. Two side-by-side 6-inch (15.24-cm) long comb structures are separated by a center divider. A copper cover (not shown) was attached with machine screws and used an indium gasket to provide intimate contact with the center divider. Coaxial lines were used to couple the signal into and out of the comb structures. A wire loop was used at the end of the structures (opposite the flange) to couple the signal from one comb structure to the other. Pump energy entered from a waveguide through a rectangular hole in

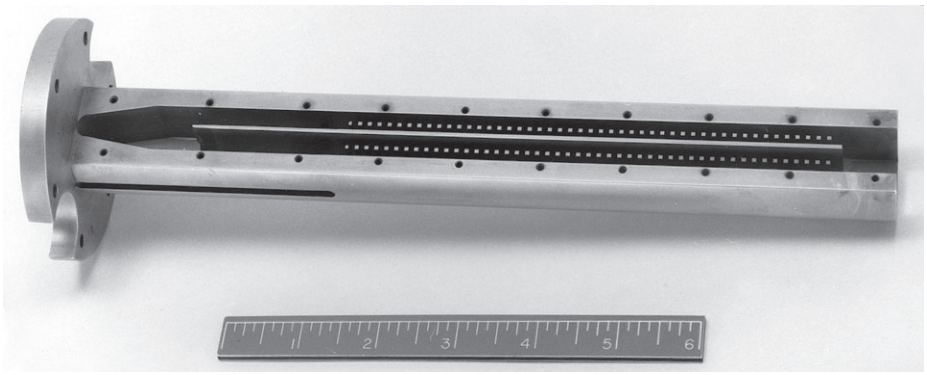

Fig. 3-7. One-piece S-band TWM comb structure (ruler for scale is in inches).

the center of the flange. The 7.26-cm (3-inch) diameter flange was bolted to the 4.5-K station of the CCR. An indium gasket between the TWM flange and the 4.5-K station provided adequate conduction.

These TWMs operated in the vacuum environment of CCRs, and the 50-mW to 100-mW heating caused by the maser pump energy was transferred from the TWM structure to the liquid helium in the 4.5-K station. The temperature difference caused by conduction through the 0.127-mm (0.005-inch) indium gasket was less than 0.01 K. The temperature difference caused by conduction through the copper maser body was about 0.1 K. The two rubies in the center of the structure were a snug fit between the center divider and the comb fingers. The two outer ruby bars were pressed against the comb structure fingers by spring tension achieved with contoured copper-plated beryllium-copper shims. The force of the outer rubies against the comb fingers caused the comb fingers to put pressure on the inner rubies, insuring intimate contact between all rubies and copper surfaces.

Properly oriented ruby of high quality was needed for maximum TWM gain. Inspection of the ruby bars was accomplished with polarized light. A ruby to be inspected was mounted between cross-polarized sheets. The crystalline structure flaws in a slab of ruby cut from a disc boule grown by the flame-fusion process are shown in Fig. 3-8. A ruby slab cut from a boule produced by the Czochralski process shows no crystalline structure flaws. The ruby was “pulled-from-melt” in the Czochralski process, and the crucible containing the molten ruby was made of iridium. The Crystal Products Division of the Union Carbide Corporation perfected the Czochralski process to grow large ruby boules of superb quality.

Early S-band TWMs and later X-band and Ku-band TWMs used polycrystalline yttrium-iron-garnet (YIG) resonance isolators. The resonant frequency of the YIG elements was determined by the magnetic field needed for ruby spin system resonance at the desired signal frequency. The shape of the YIG elements was adjusted to provide a demagnetizing factor that resulted in

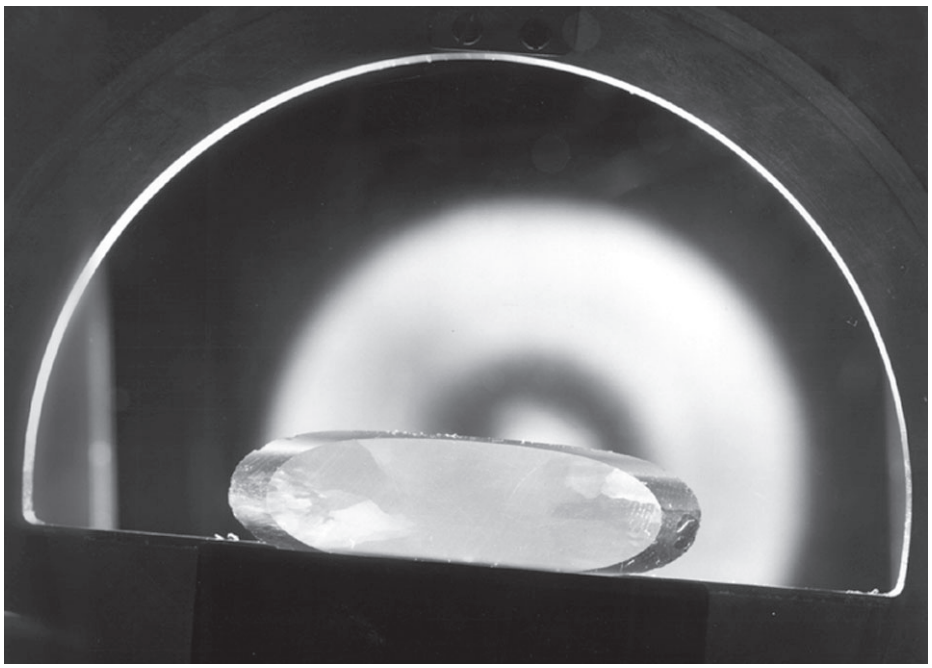

Fig. 3-8. Disc Boule ruby slab.

an internal magnetic field giving YIG resonance at the signal frequency. The internal field in a piece of YIG is determined by the saturation magnetization of the material, as well as the shape. The saturation magnetization of polycrystalline YIG is about 1750 G at room temperature and increases to a value between 2400 G and 2500 G at 4.5 K. Variations in the saturation magnetization occur, depending on the source of the YIG. The resonant frequency was also found to be dependent upon the material to which the YIG was mounted, and the adhesive used for mounting. YIG mounted directly on copper required a thickness-to-diameter ratio of 1/10 rather than 1/8 when mounted on alumina or ruby for the S-band TWMs. The difference in these thickness-to-diameter ratios shifts the YIG resonant frequency by about 400 MHz when the applied magnetic field is 2450 G.

The line width of polycrystalline YIG at 4.5 K is about 400 MHz, much wider than needed for a maser with less than 50 MHz of bandwidth. The YIG elements could be disks, or have rectangular shapes; either geometry could be made to work well. Single-crystal YIG isolators were developed for Block III and Block IV S-band masers where the regions of circular polarization in the SWS were relatively small. The volume of single-crystal YIG needed to provide adequate isolation was about 1/3 the volume of polycrystalline YIG. This reduced the forward isolator loss because the smaller pieces more closely matched the small regions of circular RF magnetic field polarization. The isolator performance improvement came at the cost of tighter tolerances. The

thickness tolerance for each piece of YIG was about ± 0.0008 mm (0.000031 inch); the measurement of dimensions was not suitable for the selection process. Doug Hofhine, a talented and patient technician, sorted and selected several thousand YIG pieces by measuring the resonant frequency of each piece in the appropriate magnetic field.

The TWM designs were optimized by using short test structures to measure and analyze the performance as a function of various changes. This cut-and-try optimization process was very efficient in terms of time and cost. Figure 3-9 shows an S-band TWM test-structure, isolators, and rubies. The comb-fingers were shaped to maximize the filling factor. Optimum isolator size and position were determined experimentally. The performance of the 7.62-cm (3-in.) test structure showed that a 30.48-cm (12-in.) slow-wave structure would give the desired gain and bandwidth. Two side-by-side structures were used to efficiently package the needed length.

The S-band TWM filling factor is at a maximum when the RF magnetic-field polarization is linear along the direction of the ruby c-axis, the direction of propagation in the case of these S-band TWMs. Large regions of linear polarization were created by the finger dimensions and spacing in the Block III S-band TWM. The optimum geometry for maximum gain leaves very small regions of circular polarization in the slow-wave structure.

The regions of circular polarization in comb-type slow-wave structures are located between the fingers, as shown in Fig. 3-10. The optimum distance from the centerline of the row of fingers towards the outside wall of the structure varies as a function of frequency.

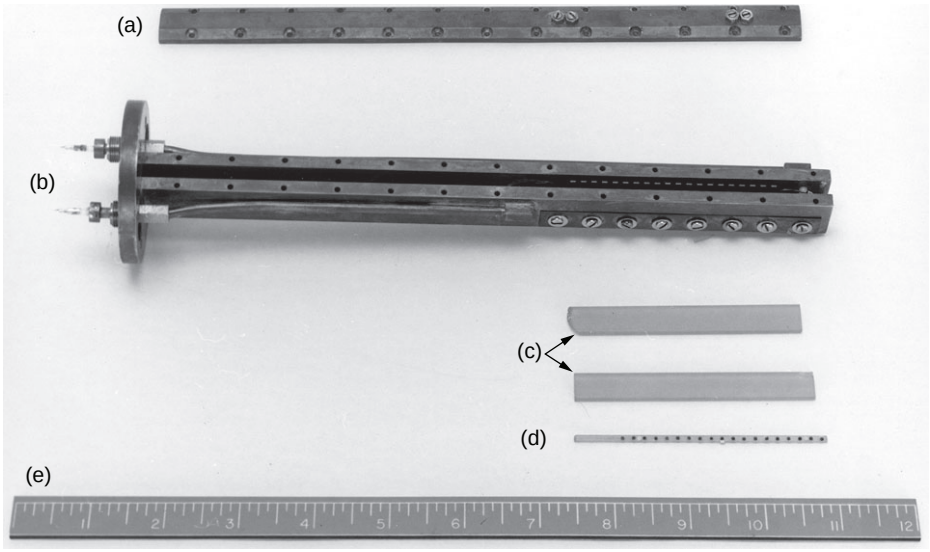

Fig. 3-9. S-band TWM test structure: (a) cover; (b) TWM test structure; (c) rubies; (d) isolator; (e) ruler for scale (inches).

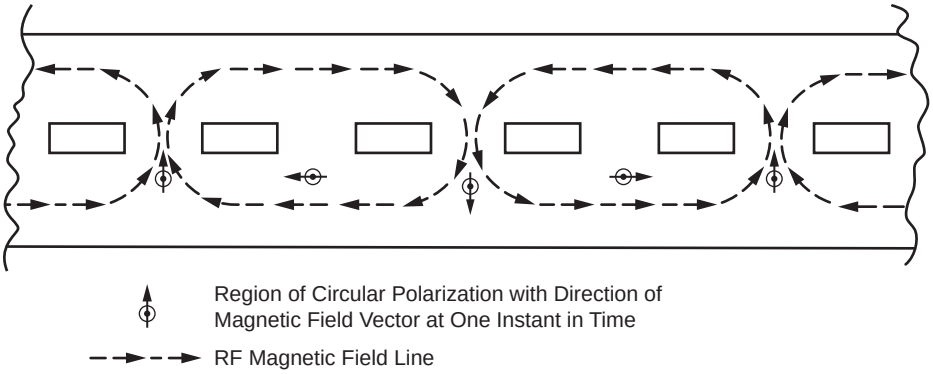

Fig. 3-10. Regions of circular polarization in a Block III S-band TWM. (Simplified RF magnetic field pattern as visualized around the base of the comb structure fingers).

At frequencies in the lower part of the slow-wave structure pass-band, the RF magnetic fields are most linear in the direction parallel to the direction of propagation. The signal phase shift from finger-to-finger approaches zero when approaching the comb-structure's low-frequency cut-off. At frequencies in the higher frequency part of the slow-wave structure pass-band, the RF magnetic fields are most linear in the direction perpendicular to the direction of propagation. The signal phase shift from finger-to-finger approaches 180 deg when approaching the comb-structure's high-frequency cut-off. The rotational sense of the circularly polarized field in the slow-wave structure is right-hand circularly polarized (RCP) on one side of the comb fingers and left-hand circularly polarized (LCP) on the other side of the comb fingers. The direction of propagation determines which side is RCP and which side is LCP.

These TWMs, using Czochralski ruby and single-crystal YIG isolators, were called Block III S-band TWMs, and 27 were built by 1973 for implementation into the DSN and NASA's S-band Tracking and Data Network (STDN) [13]. The Block III S-band TWM used a permanent magnet to supply a 2450-G (0.245-T) magnetic field. The magnet weighed about 82 kg (180 lb), and the complete maser package weighed about 204 kg (450 lb). The maser package was similar in size and shape to the Block I TWM package shown in Fig. 3-5.

A Block III S-band TWM structure was modified and used to produce a prototype of the Block IV S-band TWM. A superconducting magnet provided the 2450 G magnetic field and a short, cryogenically-cooled input transmission line reduced the noise temperature of the maser at the ambient interface to 2.1 K. The Block IV S-band TWM prototype is shown in Fig. 3-11 without the superconducting magnet. Part of the radiation shield and vacuum housing are removed to show the internal parts. This super-low-noise research and development (R&D) maser was used to (1) enable the return of Mariner 10 real-time pictures of Mercury's surface in 1974, (2) support the Inter-Cometary

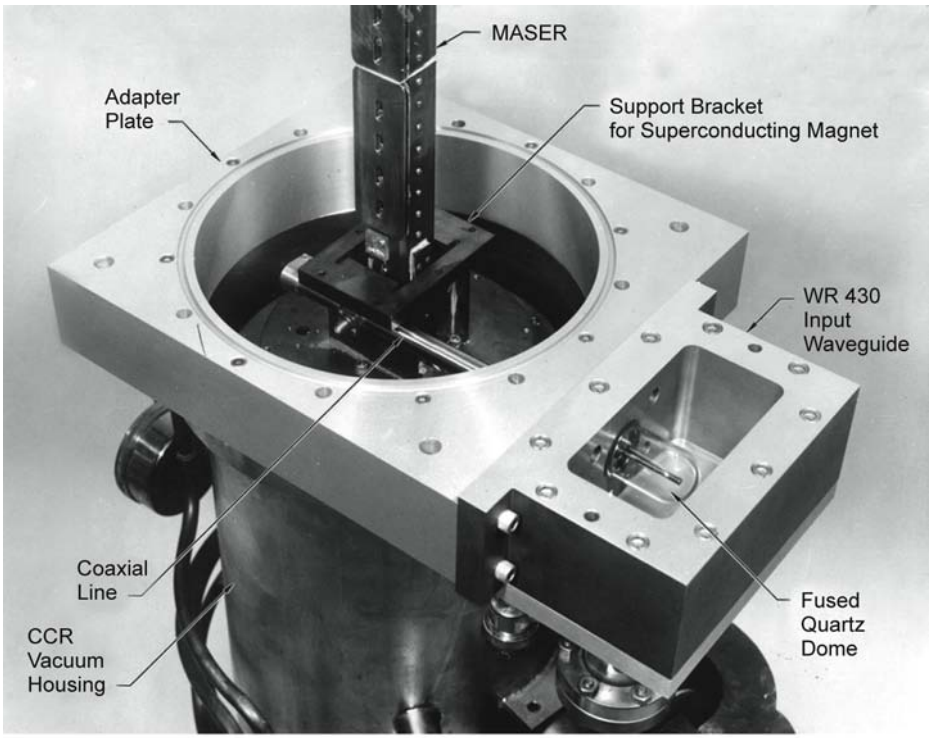

Fig. 3-11. Block IV S-band TWM prototype without superconducting magnet.

Explorer (ICE) mission at the Usuda beam-waveguide antenna in Japan [14], (3) provide radio-science support for Voyager at Usuda, and (4) support the Galileo mission at DSS-43 [15].

An S-band TWM using a half-wavelength comb structure and a box-type superconducting magnet was developed in 1985 to support the International Cometary Explorer (ICE) mission at DSS-14 (Goldstone) [14]. It had a wider instantaneous bandwidth and greater tunability than the Block III and Block IV S-band TWMs. The design was based on the development of X-band Block II TWMs between 1976 and 1980.

The development of X-band ruby masers for the DSN began long before Solar System exploration missions used the X-band deep-space-to-Earth allocation (8400 MHz to 8450 MHz). A cascaded-cavity type 8450-MHz maser was purchased from the Hughes Aircraft Company and used on the 10-m antenna at DSS-13 from 1964 to 1966 [16]. A comb-type TWM tunable from 8370 MHz to 8520 MHz was developed at JPL and used on the 64-m antenna at DSS-14 [17]. These early X-band TWMs used the 54.7-deg “push-pull” ruby orientation. The 3650-G magnetic field requirement for this orientation at X-band was provided by permanent magnets. The 5000-G field requirement for the 90-deg ruby orientation at X-band was met later with a superconducting

magnet design developed earlier for a Ku-band maser at 15.3 GHz [18]. The Ku-band maser, tunable from 14.3 GHz to 16.3 GHz was developed for use on the 64-m antenna at DSS-14 in anticipation of a deep-space-to-Earth allocation at 15.3 GHz [19].

The initial Ku-band maser plan included the possibility of using the 54.7-deg "push-pull" ruby orientation for the Ku-band TWM. Investigation of alternative maser materials was also in the plan. The investigation and tests included several materials including rutile, zinc tungstate, and emerald, with various doping agents. The results for ruby were better than the other materials [20]. Various orientations of ruby were tested with emphasis on the "push-pull" angle using the 2–3 transition for the signal and pumping the 1–3 and 2–4 transitions. These two-pump transitions are at the same frequency when the angle between the c-axis and the applied magnetic field is 54.7 deg (the energy levels are symmetrical). Tests of the push-pull pumping technique with separate pump frequencies at the 90-deg orientation showed performance inferior to the 54.7-deg orientation, but tests of push-push pumping at the 90-deg orientation (with the signal transition being the 1–2 level, and pumping the 1– 3, and 3– 4 levels) gave the best performance. The need for a higher magnetic field at this orientation was easily satisfied by use of the superconducting magnet. The superconducting magnet design for the Ku-band maser was scaled for use with X-band TWMs and the K-band (18 GHz to 26 GHz) reflected-wave masers (RWMs) developed for radio astronomy applications [21].

R&D X-band TWMs using the 90-deg ruby orientation were developed to cover tuning ranges of 7600 MHz to 8900 MHz and 7750 MHz to 8750 MHz. These TWMs were used on the 26-m antenna at DSS-13 and on the 64-m antenna at DSS-14. These TWMs served as prototypes for the Block I X-band TWM implemented to support the Viking missions in 1975 and the Voyager missions in 1977. The Block I X-band TWMs produced in excess of 45 dB gain, a noise temperature of 8 K, and an instantaneous bandwidth of more than 50 MHz, easily covering the 8400 MHz to 8440 MHz requirement [22]. The TWM with field shaping coils is shown mounted on a refrigerator in Fig. 3-12. The maser gain and bandwidth plots at five gain-control field-shaping coil settings are shown in Fig. 3-13.

These Block I X-band TWMs use push-push pumping at two frequencies near 19.2 GHz and 24.05 GHz. The Block I X-band pump klystron package with a power combiner and frequency modulator is shown in Fig. 3-14. The klystrons are frequency modulated at a rate near 100 kHz to cover the bandwidth needed. The ruby spin-relaxation times are sufficiently long to prevent the 100-kHz modulation from being transferred to the signal frequency. Each klystron is connected to a terminated circulator, used as an isolator. A waveguide that passes 24 GHz, but is cut-off at 19 GHz, passes the 24-GHz pump energy to a third three-port circulator used as a power combiner. The 19-GHz klystron is connected to the power combiner circulator at the previous

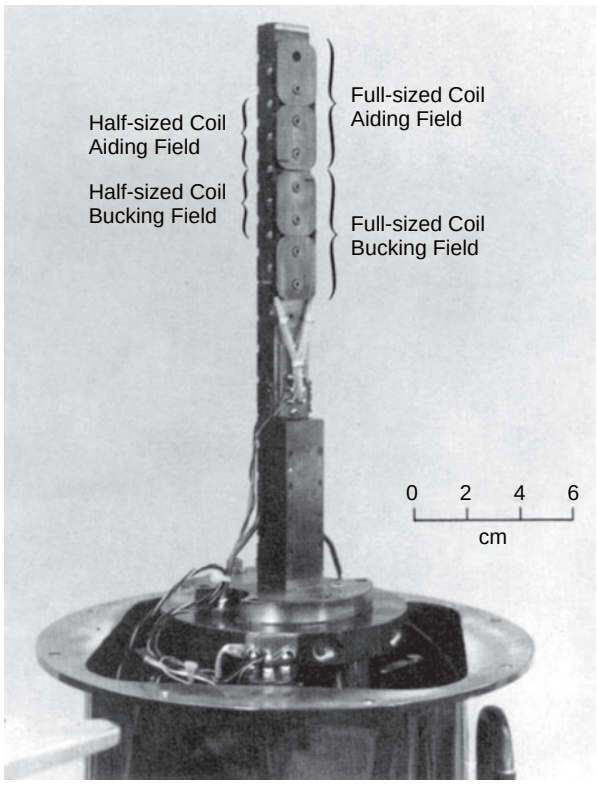

Fig. 3-12. Block-I X-band TWM with field-shaping coils mounted on refrigerator.

port, before the connection from the 24-GHz klystron. The 19-GHz pump power is reflected from the beyond-cutoff waveguide and sent on to the third port, along with the 24-GHz pump power.

The Voyager mission plans were for the two spacecraft to encounter Saturn in November 1980 and in August 1981, and for Voyager 2 to encounter Uranus in January 1986 and Neptune in August 1989. The distances from Earth would be 10 A.U. at Saturn, 19 A.U. at Uranus, and 30 A.U. at Neptune. The 115,200 bps data rate at a 5 A.U. from Jupiter translates into data rates of about 28,800 bps from Saturn, 8000 bps from Uranus, and 3200 bps from Neptune due to the square-of-the-distance penalty. Many enhancements were needed and implemented to enable the data rates of 44,800 bps from Saturn, 29,900 bps from Uranus, and 21,600 bps from Neptune that were achieved. One of the enhancements was a reduction in the system operating noise temperature of the DSN 64-m, and later 70-m, antennas. The Block II X-band masers were developed between 1976 and 1980 to contribute to this noise reduction.

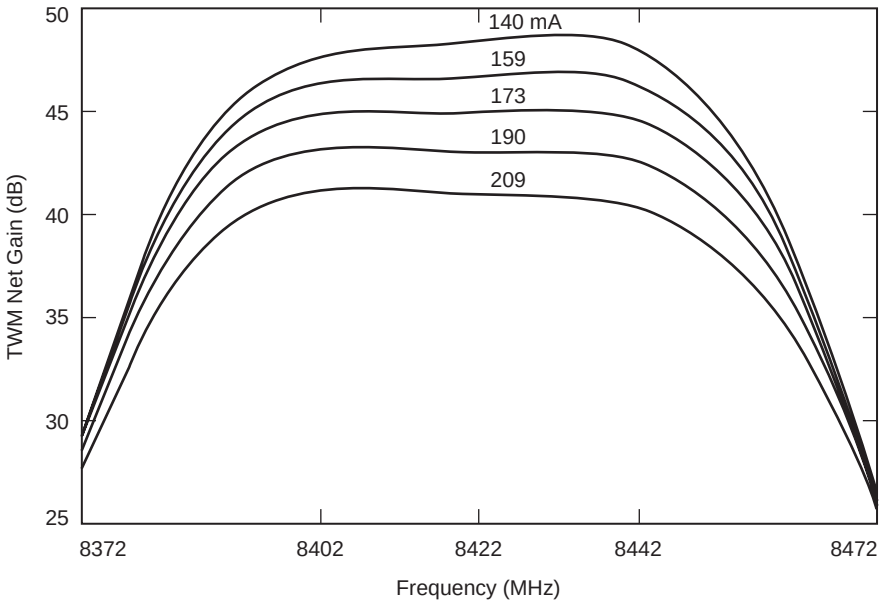

Fig. 3-13. Block-I X-band TWM gain versus frequency at five gain-control settings.

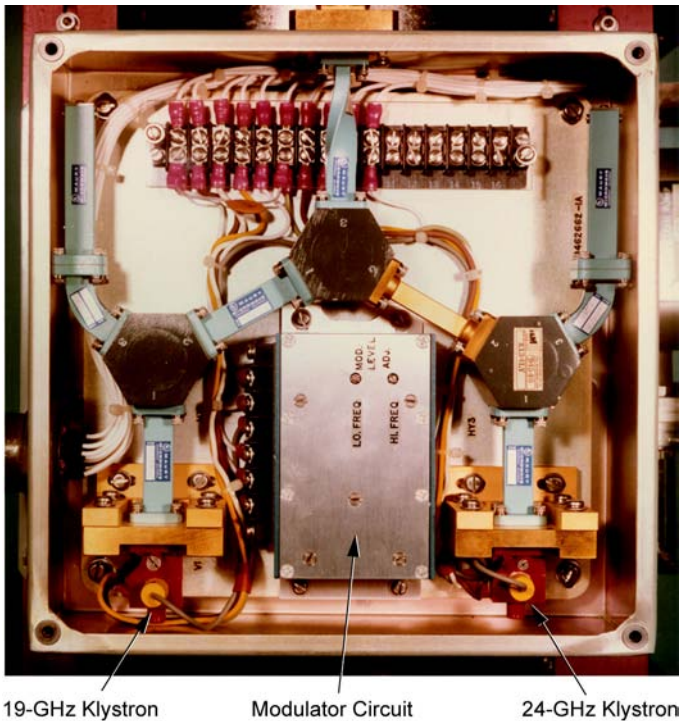

Fig. 3-14. Block-I X-band TWM pump package.

In 1980 D. L. Trowbridge reported, “Four X-band traveling-wave maser (TWM) systems with effective input noise temperatures of 3.5 K and bandwidths varying from 65 to 108 MHz have been supplied to the Deep Space Network [23]. These TWMs are used on the 64-m antennas at Deep Space Stations 14, 43, and 63 at 8420 MHz to meet the requirements of the Voyager Saturn encounter. The TWMs use shortened and cooled signal input waveguide to reduce noise and are equipped with superconducting magnets and solid state pump sources to provide the required stability performance.”

These Block II X-band TWMs were the first in a series of DSN TWMs to use ½-wavelength comb elements attached to a ruby slab in the style of a printed circuit. A goal of this design was to simplify the machining process needed to fabricate slow-wave structures with the needed precision. A new box-type of superconducting magnet was developed to accommodate a TWM volume sufficient to produce a greater gain-bandwidth product. A new staggered-height resonant isolator was developed to provide the needed bandwidth with reduced forward loss [24]. The “insides” of the TWM are shown in Fig. 3-15. The Block II TWM assembly, mounted in the superconducting magnet on the 4.5-K refrigerator is shown in Fig. 3-16. The low-noise input waveguide assembly and vacuum window are shown connected to the TWM and superconducting magnet assembly in Fig. 3-17.

Later modifications achieved a 100-MHz bandwidth for all Block II-A TWMs through the addition of a post amplifier and a gain-control attenuator.

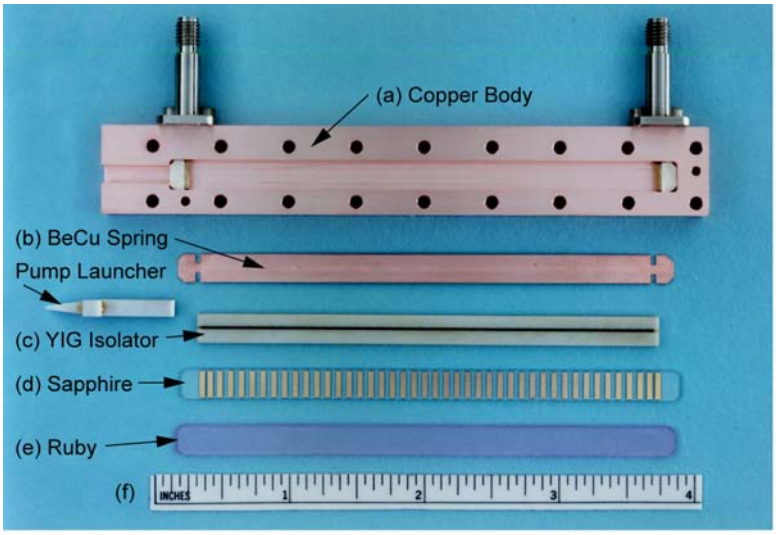

Fig. 3-15. Block III X-band TWM half-wave stripline comb structure components: (a) copper body; (b) copper-beryllium spring; (c) YIG isolator; (d) sapphire with slow-wave structure (SWS); (e) ruby; and (f) ruler for scale (in inches).

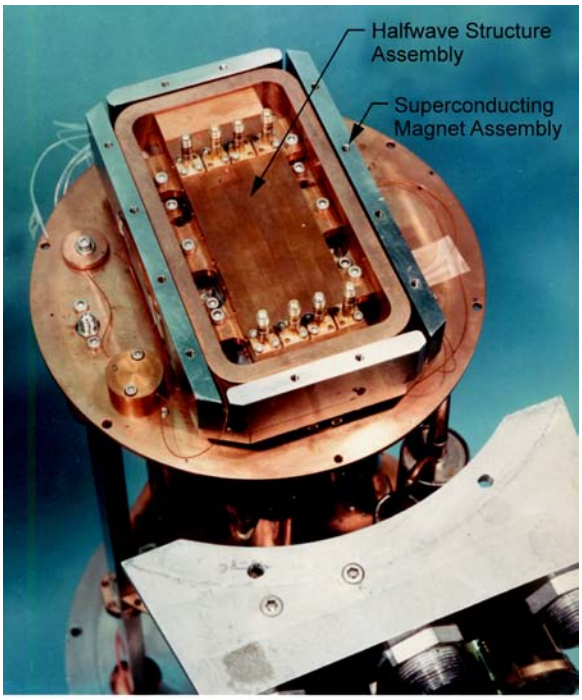

Fig. 3-16. Block II X-band TWM and superconducting magnet on 4.5-K refrigerator.

Further modifications to a Block II-A X-band TWM allowed the measurement of a total system temperature of 6.6 K with a cooled feedhorn pointed at zenith [25]. A 1.3-K effective input noise temperature was measured at the ambient interface to the TWM package. The modified Block II-A TWM was cooled to 1.6 K in superfluid helium. The X-band feedhorn was cooled, with a temperature profile that varied from about 1.6 K in the helium bath to about 300 K at the ambient interface. The ultra-low-noise X-band TWM was named the X-band ULNA. Further modifications to reduce the helium consumption rate removed the larger parts of the feedhorn from the dewar, increasing the effective input noise temperature to about 1.9 K. The X-band ULNA is used in DSS-13's Beam-Waveguide antenna to support planetary radar. The total system operating noise temperature at zenith is about 14 K in clear dry weather.

3.10 Reflected-Wave Masers

The investigation and optimization of push-push pumping techniques at 19 GHz and 24 GHz for future use with wide-bandwidth X-band TWMs was done in a well-matched ruby-filled waveguide in 1974. The well-matched ruby-filled waveguide was also tested as a reflection type amplifier in the 18- to 26.5-GHz range at temperatures between 1.9 K and 4.4 K [26]. The 0.178 cm

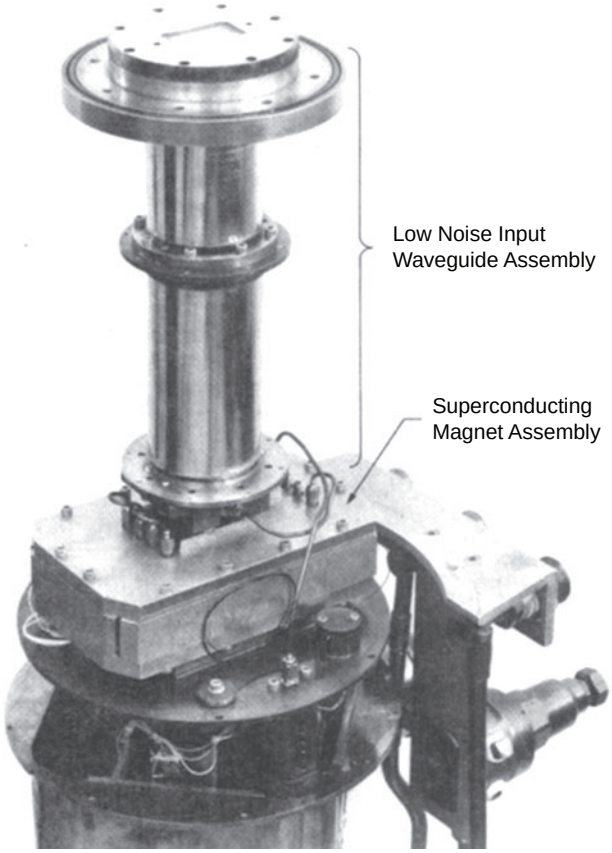

Fig. 3-17. Block-II X-band TWM with input waveguide assembly.

high by 0.356 cm by 5.08 cm (2 in.) long ruby filled section was matched to a standard WR42 (18-GHz to 26.5-GHz) waveguide with a 7.62-cm long tapered matching section. Magnetic shims were added to broaden the ruby linewidth and reduce the gain of the amplifying section to avoid regeneration. Gain values between 7 dB and 7.7 dB were observed across a 285-MHz bandwidth near 24.4 GHz at 4.4 K. Gain values between 15 dB and 17 dB were observed across a 250-MHz bandwidth near 24 GHz at 1.9 K. The ruby-filled waveguide, combined with a circulator and a pump source, formed a simple amplifier stage that could be tuned electronically across the entire 18-GHz to 26.5-GHz range. Several such stages used in series could achieve high gain with wide bandwidth.

A reflected-wave maser (RWM) was developed for use between 9 and 10 GHz with the support of grants from the California Institute of Technology President's Fund and the National Science Foundation. The maser group at JPL, and Professor Sheldon Schultz and Larry Flesner of the Physics

Department at the University of California, San Diego (UCSD), in La Jolla, California worked together on this task [27]. This maser improved the sensitivity of a transmission electron spin resonance spectrometer used in the UCSD Physics Laboratory.

A technology sharing contract between JPL and the National Radio Astronomy Observatory of the Associated Universities Inc. (NRAO, AUI) resulted in the development of "A Reflected-Wave Ruby Maser with K-Band Tuning Range and Large Instantaneous Bandwidth" [21]. This first K-band RWM was used on the NRAO 43-m (140-foot) diameter antenna at Greenbank, West Virginia. The effective input noise temperature of the maser-receiver was 13 K ±2 K, and the instantaneous bandwidth was 250 MHz near the center of the tuning range.

Craig Moore of NRAO, who had worked at JPL with the maser group to develop this RWM, later improved the performance of the K-band RWM, increasing the instantaneous bandwidth to more than 500 MHz. This bandwidth improvement was accomplished with a superconducting magnet that provided the needed magnetic field shape across the entire 15.24-cm (6-in.) length of the RWM structure [28]. Craig Moore shared his new magnet design with JPL, and subsequent K-band RWMs were built for, and in cooperation with:

1) Caltech's Owens Valley Radio Observatory,
2) Professor David Wilkinson and Dale Fixsen of Princeton University and Sam Gulkis of JPL for a balloon-borne maser measurement of the large-scale anisotropy of the cosmic background radiation, and
3) The Max Planck Institute for Radio Astronomy.

K-band RWMs were also used on the DSN's 70-m antennas to support radio astronomy applications. Additional maser-technology sharing contracts enabled work on masers for radio and radar astronomy for the Arecibo radio telescope in Puerto Rico and for the Haystack Observatory in Massachusetts.

An RWM was developed for the 32-GHz applications [29]. The Ka-band RWM used eight channels of ruby filled waveguide and a box-type 1.18-T (11,800-G) superconducting magnet, similar to the geometry of the magnet developed for the Block II X-band masers. The Ka-band RWM was cooled by a closed-cycle helium refrigerator like those used for other masers in the DSN. The maximum bandwidth achieved was 400 MHz with 21 dB of net gain. Four impact avalanche and transit time (IMPATT) oscillators, each providing about 100 mW near 66.4 GHz, were used to pump the maser. A pump power of 400 mW was not adequate to pump and saturate the relatively large volume of ruby across a 400-MHz bandwidth. Reducing the pump frequency modulation bandwidth increased the net gain to 40 dB with a 150-MHz bandwidth. At 40 dB gain, the Ka-band RWM demonstrated an effective input noise temperature of about 13 K at the ambient waveguide interface.

3.11 Ka-Band and the Return to Cavity Masers

Establishment of Ka-band allocations for deep-space-to-Earth (downlink) telecommunications from 31.8 GHz to 32.3 GHz and Earth-to-deep-space (uplink) telecommunications from 34.2 GHz to 34.7 GHz created 500-MHz wide bands for future Solar System exploration missions. Telecommunications and navigation needs would be served well by DSN antenna systems having high efficiency and low-noise performance at Ka-band. Low-noise amplifier development at Ka-band began in the 1980s.

Attempts to develop ¼ wavelength and ½ wavelength comb-type traveling-wave masers at 32 GHz were not successful. The earlier comb-type slow-wave structures developed for S-band, X-band, and Ku-band showed an increasing demand for precise dimensions as the frequency increased. It was not a surprise that comb structure tolerances would be very difficult and possibly beyond our ability to meet.

The experience with comb-type slow-wave structures and the RWM at 32 GHz convinced us of the need to find a better approach for building Ka-band masers. The Mars Observer spacecraft would use the X-band, near 8420 MHz, for downlink telemetry from Mars. A simple, low-power Ka-band transmitter was planned for a Ka-Band Link Experiment (KaBLE) between Mars Observer and the new 34-m beam-waveguide DSN research antenna at DSS-13. The KaBLE downlink was created by multiplying the X-band downlink frequency by a factor of 4, producing signals near 33.68 GHz. The Mars Observer downlink frequency would shift across a 5-MHz range, from below 8420 MHz to above 8420 MHz, depending on the spacecraft mode. The spacecraft mode would be dependent upon the use of an uplink for the two-way mode, or it would automatically switch to the one-way mode when the spacecraft was not locked to an uplink. The Ka-band maser would need to cover a bandwidth somewhat greater than 40 MHz, centered at 33.68 GHz.

A two-cavity maser design was selected and developed to support the Mars Observer KaBLE at frequencies near 33.68 GHz [5]. Figure 3-18 shows a schematic diagram of the dual-cavity Ka-band maser. Each cavity was composed of a piece of ruby with an electrical length of 1.5 wavelengths in a 2.54 mm × 1.27 mm copper waveguide. The physical length of the ruby is about 3.8 mm. Each ruby extends about 0.3 mm into a reduced height WR30 signal waveguide that connects to a circulator. The circulators are commercially available WR28 waveguide units. Impedance transformers using 1/4 wavelength steps are used to match the WR28 to the reduced height WR30 waveguides. The external and loaded *Q* of each ruby-filled cavity is determined by the length of the ruby extension into the reduced-height WR30 signal waveguide. 69.5-GHz pump energy is supplied through the 2.54 mm × 1.27 mm waveguide connected to the ruby-filled section at the end that is opposite the signal waveguide connection.

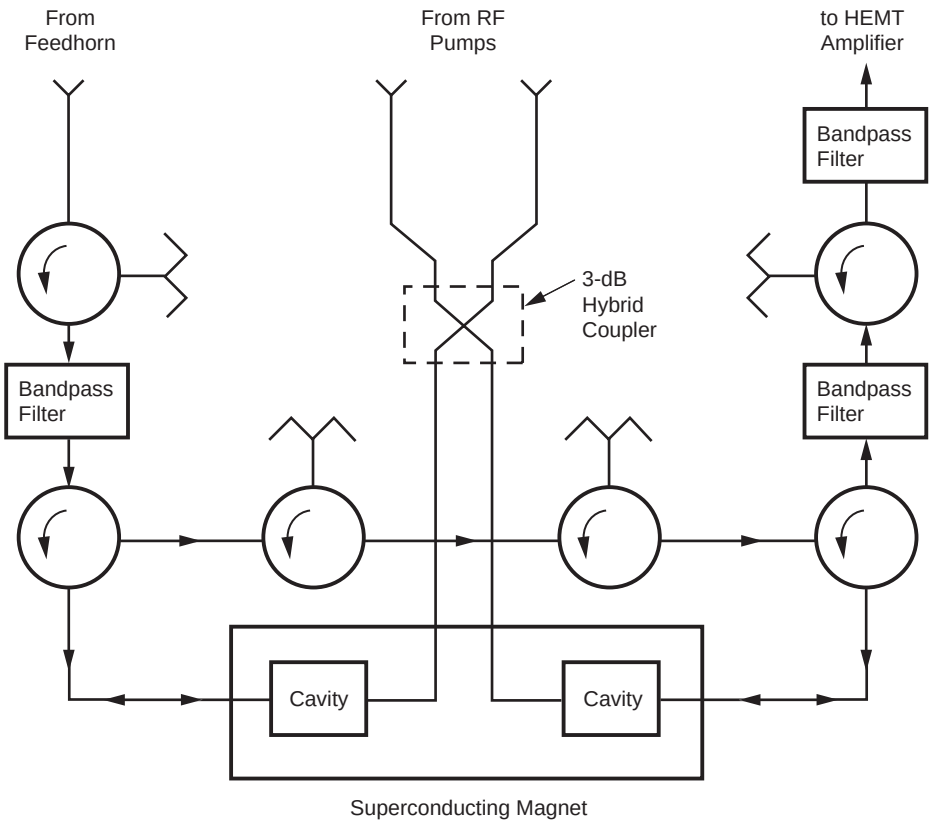

Fig. 3-18. Dual-cavity Ka-band maser schematic diagram.

The ruby-filled cavities were mounted inside a 1.24-T (12, 400-G) circular magnet, somewhat different in shape than the box-type magnet used for the 32-GHz RWM. The roughly square shape of the dual-cavity housing could have used a square superconducting coil, but a slightly larger circular coil was chosen to simplify the winding process. The niobium-titanium superconducting wire, surrounded by an iron alloy with high permeability (Hyperco-27), was similar to previously used box magnets in the respect that these geometries do not depend upon the use of additional superconducting shielding (usually niobium-tin) to prevent straying magnetic fields that destroy the magnetic-field uniformity. The feedhorn, connecting waveguide assemblies, and cryogenically cooled HEMT follow-up amplifiers were all located in the helium dewar with the maser.

The concentric liquid-helium double dewar was purchased from International Cryogenics, Inc. (Indianapolis, Indiana). Reduction of the vapor pressure above the liquid helium in the 22-liter inner dewar reduced the temperature of the super-fluid helium to 1.5 K. The vapors were used to cool

the feedhorn. A capillary tube assembly from the outer 80-liter 4.2-K dewar was designed to allow for continuous replenishment of the 1.5-K super-fluid helium. This configuration allowed for refilling helium without interrupting maser operation.

Two Hughes 47134H-1110 IMPATT Oscillators each provided 100-mW pump power near 69.5 GHz. These were frequency modulated across a 170-MHz bandwidth at a rate of 20 kHz. The electronic gain of the maser is 28 dB, the net gain is 25 dB, the inversion ratio is 2.0, and the –3 dB bandwidth is 85 MHz. The gain (with pumps on) and ruby absorption (with pumps off) is shown as a function of frequency in Fig. 3-19. The gain can be adjusted for higher or lower values with trim coils that change the magnetic field gradient, thereby artificially increasing or decreasing the ruby line-width and the maser's bandwidth.

A 5 K ±1 K effective input noise temperature was measured at the maser package feedhorn aperture. The uncertainty is due to the tolerance on the sky brightness temperature during the measurement. Surface temperature and relative humidity measurements were used to model the atmosphere's contribution. The maser's measured effective input noise temperature agrees well with computations of 3 K for the maser in the 1.5 K bath at the input to the first circulator, 0.3 K for cooled waveguide components, and 1.7 K for the feedhorn and Kapton window loss. The effective noise temperature of each cavity is calculated to be 2.2 K at an electronic gain of 14 dB and a net gain of 13.5 dB.

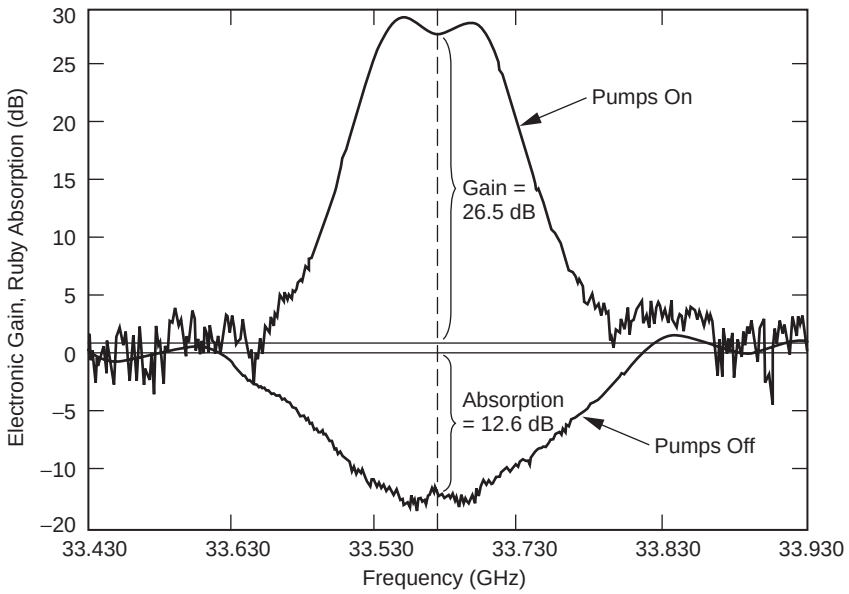

Fig. 3-19. Electronic gain with RF pumps on, and ruby absorption with RF pumps off, for the dual-cavity 33.68-GHz (Ka-band) maser.

3.12 Analysis of Maser Designs

As discussed above, construction of Ka-band traveling-wave masers (TWM) using comb type slow-wave structures (SWS) is not practical. A maser employing several stages of reflection type coupled waveguide cavities or a traveling-wave design using coupled cavities is considered to be the best approach to achieve instantaneous bandwidths of 500 MHz. Computer programs capable of modeling the passive characteristics of such structures have existed for some time [30]. However, the authors are not aware of any program capable of modeling the ruby gain. Development of such a program was undertaken at JPL.

The approach was based on the well-known mode-matching technique. A concise description of the waveguide mode-matching formulation can be found in reference [31]. The results of the program are the microwave scattering parameters. By using a generalized scattering matrix formulation, the interaction between waveguide cavities includes higher order modes if present. Antenna engineers at JPL developed a mode-matching program for the analysis of corrugated feedhorns [32]. This program was the starting point for the maser design program. The effect of the resonant spin system in the ruby was added by appropriately modifying the propagation constants of the waveguide modes used in the mode-matching formulation.

Each waveguide mode propagation constant is given by

$$\gamma^2 = k_c{}^2 - k^2 = k_c{}^2 - \omega^2 \mu_{\text{eff}} \varepsilon_{\text{eff}} \tag{3.12-1}$$

where $k_c{}^2$ is the square of the cut-off wavenumber, determined by the cross sectional dimensions of the waveguide and k^2 is the square of the wave vector magnitude. μ_{eff} and ε_{eff} are the effective scalar permeability and permittivity of the material filling the waveguide, and ω is the angular frequency. The impedance of each H-mode and E-mode used in the mode-matching analysis is also modified according to

$$Z_H = \frac{j\omega\mu_{\text{eff}}}{\gamma} \quad \text{and} \quad Z_E = \frac{\gamma}{j\omega\varepsilon_{\text{eff}}} \tag{3.12-2}$$

In his analysis of the traveling wave maser, Siegman [6] calculates the change in the propagation constant due to changes in the material in which the slow wave circuit is embedded. Siegman's result for the change in propagation constant, due to a complex susceptibility in an isotropic magnetic material, is given by

$$\Delta\gamma = \beta - \beta_o - j\alpha = \frac{\omega}{2v_g}(\chi' - j\chi'') \tag{3.12-3}$$

In this equation, β, β_o, α are the phase constant in the presence of magnetic resonance, the phase constant without magnetic resonance, and the attenuation constant with magnetic resonance. The attenuation constant in the absence of magnetic resonance is assumed to be zero, i.e., $\alpha_o = 0$. Siegman's analysis shows that the effect of the ruby spin system on the wave vector of the medium is described by the magnetic susceptibility. Following Siegman, we assume the analytic expression will remain valid within some limits as $\mu, \varepsilon, \gamma, k$ become complex quantities.

Since the magnetic susceptibility of many maser materials (ruby for example) is a tensor quantity, a technique is required to appropriately reduce this tensor quantity to an equivalent complex scalar. (In our program, the permittivity tensor is replaced by an equivalent frequency independent complex scalar. This is simpler than the permeability since no gain or resonant behavior is involved with the permittivity).

Lax and Button investigated the change in the propagation constant of an infinite waveguide of arbitrary cross section loaded with a medium which fills it wholly or partially in the transverse plane, but is uniform in the axial direction [33]. They found,

$$\gamma + \gamma_o{}^* = \frac{j\omega\int(\mathbf{H_0}^* \cdot \Delta\bar{\bar{\mu}} \cdot \mathbf{H_1}) + (\mathbf{E_0}^* \cdot \Delta\bar{\bar{\varepsilon}} \cdot \mathbf{E_1})dS}{\int(\mathbf{E_0}^* \times \mathbf{H_1} + \mathbf{E_1} \times \mathbf{H_0}^*)dS} \tag{3.12-4}$$

where $\Delta\bar{\bar{\mu}}$ and $\Delta\bar{\bar{\varepsilon}}$ is the change in the permeability and permittivity tensors, respectively due to the perturbation. The propagation constants γ and γ_o are with and without the dielectric material. $\mathbf{H_0}$, $\mathbf{H_1}$ and $\mathbf{E_0}$, $\mathbf{E_1}$ are the unperturbed and perturbed microwave magnetic and electric fields, respectively. The integrations are over the waveguide cross-section. Because the waveguide cross section was arbitrary, we are effectively determining the change in the propagation constant due to the change in the wave vector of the medium, albeit surrounded by a metallic enclosure.

In our case, we choose the "unperturbed waveguide" to be that of the ruby filled waveguide without a resonant spin system. Since there is no change in the permittivity, we can set $\Delta\bar{\bar{\varepsilon}} = 0$. Since the ruby spin system is dilute, we can approximate the perturbed fields by the unperturbed fields. Thus, Eq. (3.12-4) simplifies to,

$$\gamma + \gamma_o^* = \frac{j\omega \iint \mathbf{H_0}^* \cdot \overline{\overline{\Delta\mu}} \cdot \mathbf{H_0} ds}{\int (\mathbf{E_0}^* \times \mathbf{H_0} + \mathbf{E_0} \times \mathbf{H_0}^*) ds} \tag{3.12-5}$$

The denominator is four times the power flow down the guide, which is equal to the energy stored times the group velocity. In the numerator $\overline{\overline{\Delta\mu}}$ can be replaced by $\mu_o \overline{\overline{\chi}}$. Thus,

$$\gamma + \gamma_o^* = \frac{j\omega\mu_o \iint \mathbf{H_0}^* \cdot (\overline{\overline{\chi}}) \cdot \mathbf{H_0} ds}{4 v_g \iint \frac{\mu_o \mathbf{H_0}^* \cdot \mathbf{H_0}}{2} ds} \tag{3.12-6}$$

where we have expressed the energy storage in terms of the magnetic field.

For an anisotropic material, the susceptibility tensor can be broken into real and imaginary parts.

$$\overline{\overline{\chi}} = \overline{\overline{\chi'}} - j\overline{\overline{\chi''}} \tag{3.12-7}$$

They are given in terms of the full susceptibility tensor by

$$\overline{\overline{\chi'}} = \frac{1}{2}(\overline{\overline{\chi}} + \overline{\overline{\chi_t}}^*) \quad \text{and} \quad -j\overline{\overline{\chi''}} = \frac{1}{2}(\overline{\overline{\chi}} - \overline{\overline{\chi_t}}^*) \tag{3.12-8}$$

where $\overline{\overline{\chi_t}}^*$ is the hermitian conjugate of $\overline{\overline{\chi}}$.
Therefore, we can write Eq. (3.12-6) as

$$\gamma + \gamma_o^* = \frac{j\omega}{2 v_g} \frac{\iint \mathbf{H_0}^* \cdot (\overline{\overline{\chi'}} - j\overline{\overline{\chi''}}) \cdot \mathbf{H_0} ds}{\iint \mathbf{H_0}^* \cdot \mathbf{H_0} ds} \tag{3.12-9}$$

Equating the imaginary parts of the propagation constants yields

$$(\beta - \beta_o) = \frac{\omega}{2 v_g} \frac{\iint \mathbf{H_0}^* \cdot (\overline{\overline{\chi'}}) \cdot \mathbf{H_0} ds}{\iint \mathbf{H_0}^* \cdot \mathbf{H_0} ds} \tag{3.12-10}$$

Equating the real parts (assuming $\alpha_o = 0$) yields

$$\alpha = \frac{\omega}{2v_g} \frac{\iint \mathbf{H_0}^* \cdot (\overline{\overline{\chi''}}) \cdot \mathbf{H_0} ds}{\iint \mathbf{H_0}^* \cdot \mathbf{H_0} ds} \tag{3.12-11}$$

Comparing this to Eq. (3.12-3), we find that the effective scalar susceptibility corresponding to the tensor susceptibility is given by

$$\chi'_{\text{eff}} - j\chi''_{\text{eff}} = \frac{\iint \mathbf{H_0}^* \cdot \left(\overline{\overline{\chi'}} - j\overline{\overline{\chi''}}\right) \cdot \mathbf{H_0} ds}{\iint \mathbf{H_0}^* \cdot \mathbf{H_0} ds} \tag{3.12-12}$$

For the case of ruby, the full susceptibility tensor is given by

$$\overline{\overline{\chi}} = \frac{\pi\mu_o}{\text{h}} (\text{g}\beta)^2 (n_i - n_j) \{h(f - f_o) - jg(f - f_o)\} \overline{\overline{S}} \tag{3.12-13}$$

where

h = Planck's constant, 6.626×10^{-34} joule-second (J-s)

μ_0 = permeability of free space, 1.26×10^{-6} newtons/(amperes)^2 (N/A^2)

g = g-factor of the free electron 2.0023, (unitless value)

β = Bohr magnetron, 9.27×10^{-24} joules/tesla (J/T)

Also, $(n_i - n_j)$ is the difference in the number of spins per unit volume in states i and j. The line-shape functions describe the variation of the susceptibility away from the resonant frequency f_o. Two line-shape functions are used and are denoted by $g(f - f_o)$ and $h(f - f_o)$, respectively. They are given by

$$h(f - f_o) = \frac{4(f_o - f)}{\pi(\Delta f_L)^2 + 4\pi(f - f_o)^2} \tag{3.12-14}$$

$$g(f - f_o) = \frac{2\Delta f_L}{\pi(\Delta f_L)^2 + 4\pi(f - f_o)^2} \tag{3.12-15}$$

The quantity Δf_L is the linewidth of the ruby. The quantity $\overline{\overline{S}}$ is called the spin tensor, and it must be evaluated using the methods of quantum mechanics. The anisotropic nature of $\overline{\overline{\chi}}$ is contained within it. The spin tensor is given by,

$$\overline{\overline{S}} = \vec{S}^{ij}\left(\vec{S}^{ij}\right)^{*}, \tag{3.12-16}$$

where $\vec{S}^{ij}\left(\vec{S}^{ij}\right)^{*}$ is a dyadic product formed using the quantum mechanical spin vector operator. The indices *i*, *j* refer to the quantum states between which a given transition takes place. They can refer to a signal, pump or to an idle transition. Using the Dirac bra-ket notation, the states are represented by $< i |$ and $| j >$. The spin vector operator is given by

$$\begin{aligned}\vec{S}^{ij} &= \langle i|\vec{S}|j\rangle \\ &= \langle i|S_x\hat{x} + S_y\hat{y} + S_z\hat{z}|j\rangle \\ &= \langle i|S_x|j\rangle\hat{x} + \langle i|S_y|j\rangle\hat{y} + \langle i|S_z|j\rangle\hat{z}\end{aligned} \tag{3.12-17}$$

or

$$\vec{S}^{ij} = S_x{}^{ij}\hat{x} + S_y{}^{ij}\hat{y} + S_z{}^{ij}\hat{z} \tag{3.12-18}$$

Dropping the superscript, *ij*, we can write

$$\overline{\overline{S}} = \vec{S}\left(\vec{S}\right)^{*} = \begin{pmatrix} S_x \\ S_y \\ S_z \end{pmatrix}\begin{pmatrix} S_x{}^{*} & S_y{}^{*} & S_z{}^{*} \end{pmatrix} = \begin{pmatrix} S_xS_x{}^{*} & S_xS_y{}^{*} & S_xS_z{}^{*} \\ S_yS_x{}^{*} & S_yS_y{}^{*} & S_yS_z{}^{*} \\ S_zS_x{}^{*} & S_zS_y{}^{*} & S_zS_z{}^{*} \end{pmatrix} \tag{3.12-19}$$

In this form, $\overline{\overline{S}}$ is hermitian. Using Eq. (3.12-8), it can be shown that

$$\overline{\overline{\chi'}} = \frac{\pi\mu_o}{\mathrm{h}}(\mathrm{g}\beta)^2\left(n_i - n_j\right)h\left(f - f_o\right)\overline{\overline{S}} \tag{3.12-20}$$

and

$$\overline{\overline{\chi''}} = \frac{\pi\mu_o}{\mathrm{h}}(\mathrm{g}\beta)^2\left(n_i - n_j\right)g\left(f - f_o\right)\overline{\overline{S}}. \tag{3.12-21}$$

A concise description of the low-lying quantum states, $< i |$, $| j >$ is made possible through the concept of an “effective spin Hamiltonian”. This approach includes such effects as the Zeeman splitting of the quantum states due to applied magnetic fields. It also describes the splitting of energy levels due to the electrostatic field of surrounding atoms. An excellent discussion of this concept can be found in [34]. The eigenvalues of the spin Hamiltonian matrix

are the energies of the discrete quantum states available to the spins. The difference in energies divided by Planck's constant determines the resonant transition frequencies. The eigenvector associated with an eigenvalue is a representation of the quantum state having that energy.

The presence of the crystalline electric fields makes the form of the spin Hamiltonian dependent on the orientation of the coordinate system. Taking ruby as an example, if the crystal c-axis is chosen along the z-direction, then the spin Hamiltonian, H_s, is given by

$$H_s = \mathrm{g}_1 \beta H_z S_z + \mathrm{g}_2 \beta \left(H_x S_x + H_y S_y \right) + \mathrm{D}\left[{S_z}^2 - \frac{1}{3} S(S+1) \right] \qquad (3.12\text{-}22)$$

Here g_1 and g_2 are spectroscopic splitting factors, β is the Bohr magneton, and $\overrightarrow{H_{dc}} = (H_x, H_y H_z)$ is the applied static magnetic field.

Personnel at Bell Telephone Laboratories derived a Hamiltonian for which the z-axis is along the applied static magnetic field [35]. The ruby crystal c-axis is specified by the polar angle, θ, with respect to the dc magnetic field and an azimuthal angle, φ, with respect to the x-axis. Their result is

$$\begin{aligned} H_s = & \left(\mathrm{g}_1 \cos^2\theta + \mathrm{g}_2 \sin^2\theta \right) \beta H_z S_z \\ & + \mathrm{D}\left(\cos^2\theta - 1/2 \sin^2\theta \right) \left[{S_z}^2 - 1/3 S(S+1) \right] \\ & + \mathrm{D}(1/2)(\cos\theta \sin\theta) \left[e^{-i\varphi} \left(S_z S_+ + S_+ S_z \right) + e^{i\varphi} \left(S_z S_- + S_- S_z \right) \right] \\ & + \mathrm{D}(1/4) \sin^2\theta \left(e^{-2i\varphi} {S_+}^2 + e^{2i\varphi} {S_-}^2 \right) \end{aligned} \qquad (3.12\text{-}23)$$

Here $S_+ = S_x + iS_y$, $S_- = S_x - iS_y$, and $i = \sqrt{-1}$. We use the values for the spectroscopic splitting factors $\mathrm{g}_1 = 1.9817$ and $\mathrm{g}_2 = 1.9819$, and the zero-field splitting $\mathrm{D} = -3.8076 \cdot 10^{-17}$ ergs, published by the National Bureau of Standards [36].

The coordinate system appropriate to this Hamiltonian is shown in Fig. 3-20. From the point of view of maser design analysis, it makes more sense to fix the direction of the applied field and let the direction of the ruby c-axis be unrestricted. The result is a more complex expression for the spin Hamiltonian. However, since a digital computer performs the calculation, the additional complexity is not a concern. Eq. (3.12-22) can be shown to be almost exactly equal to Eq. (3.12-23). We have neglected terms involving the difference between g_1 and g_2 because they are nearly equal.

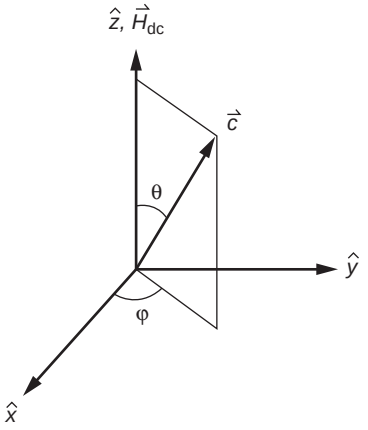

Fig. 3-20. Coordinate system for calculation of ruby spin Hamiltonian.

The components of the spin vector operator, S_x, S_y, S_z are matrices given below. The quantity D represents one half of the "zero-field splitting." This is the initial splitting of the four quantum states of a spin 3/2 chromium ion into two doublets in the absence of a magnetic field. The quantity $S(S+1)$ is the eigenvalue of the operator $S^2 = S_x{}^2 + S_y{}^2 + S_z{}^2$.

In addition to choosing a coordinate system for the spin Hamiltonian, we must choose a representation for the spin operators. This means choosing a set of base states in terms of which the spin quantum states can be expressed. The usual choice for a spin system is the set of states that are simultaneous eigenstates of the total angular momentum squared and the projection of the angular momentum along some axis, usually the z-axis. In this representation, the matrices representing S^2 and S_z are diagonal. We adopt this convention. For a spin S = 3/2 system, such as the Cr^{+3} ion in ruby, they are given as 4-by-4 matrices. In particular,

$$S^2 = 15/4 \cdot \begin{bmatrix} 1 & 0 & 0 & 0 \\ 0 & 1 & 0 & 0 \\ 0 & 0 & 1 & 0 \\ 0 & 0 & 0 & 1 \end{bmatrix} \qquad S_z = 1/2 \cdot \begin{bmatrix} 3 & 0 & 0 & 0 \\ 0 & 1 & 0 & 0 \\ 0 & 0 & -1 & 0 \\ 0 & 0 & 0 & -3 \end{bmatrix} \tag{3.12-24}$$

In this representation, the matrices representing the spin operators S_x and S_y are given by

$$S_x = 1/2 \cdot \begin{bmatrix} 0 & \sqrt{3} & 0 & 0 \\ \sqrt{3} & 0 & 2 & 0 \\ 0 & 2 & 0 & \sqrt{3} \\ 0 & 0 & \sqrt{3} & 0 \end{bmatrix} \text{ and}$$

$$S_y = 1/2 \cdot \begin{bmatrix} 0 & -\sqrt{3}i & 0 & 0 \\ \sqrt{3}i & 0 & -2i & 0 \\ 0 & 2i & 0 & -\sqrt{3}i \\ 0 & 0 & \sqrt{3}i & 0 \end{bmatrix} \qquad (3.12\text{-}25)$$

In summary, knowing the spin Hamiltonian given in Eq. (3.12-23), the eigenvectors can be calculated. With the eigenvectors and the spin operators given in Eqs. (3.12-24) and (3.12-25), we can calculate the spin vector given in Eq. (3.12-17). With the spin vector, the spin tensor is calculated using Eq. (3.12-19). With the spin tensor, the real and imaginary parts of the susceptibility tensor are calculated using Eqs. (3.12-20) and (3.12-21). Finally, knowing the RF magnetic field in the regions containing ruby allows the effective scalar susceptibility to be evaluated using Eq. (3.12-12). (The RF magnetic field is calculated from the scattering parameters using the same mode-matching program). This allows the effective magnetic permeability to be calculated using

$$\mu_{\text{eff}} = \mu'_{\text{eff}} - j\mu''_{\text{eff}} = \mu_o \left(1 + \chi'_{\text{eff}} - j\chi''_{\text{eff}}\right) \qquad (3.12\text{-}26)$$

Finally, the effective permeability is used in Eq. (3.12-1) to determine the propagation constant.

The program has given good agreement with experiments. The K-band and Ka-band RWMs were appropriate for analysis by this program, and the analysis results were consistent with the previously measured performance. Designs using waveguide cavities filled with ruby, having the same loaded-Q as the S-band coaxial cavities used in the early JPL cavity masers were analyzed. Again, the results were consistent with the performance measured 40 years before this analysis tool was developed.

A Ka-band waveguide coupled-cavity maser design was optimized by analyzing various combinations of impedance transformers, irises, empty cavities, and a ruby filled cavity [37]. The program analyses these designs but does not generate the design. The design must be produced based on the designer's knowledge and use of other microwave design tools. The process might be described as automated cut-and-try, with no actual fabrication taking

place. When the analysis of any given design shows the desired result, it is then time for fabrication.

Fabrication of the coupled-cavity design was completed, and subsequent RF measurements showed performance that was not as predicted by the analysis. The analysis program was then used to make changes to obtain the same results as produced by the RF measurements. One change was needed in the impedance matching transformer. The height of one step was changed by 0.076 mm, about 2 percent of the 3.556-mm empty waveguide height. Inspection of the structure showed that there had been a machining error of the size and location, in the impedance transformer, just as indicated by the analysis program.

Subsequent Ka-band maser designs were produced with the goal of simplifying the machining process. A cascaded-cavity TWM design was developed [38]. A drawing of the design is shown in Fig. 3-21. A unique

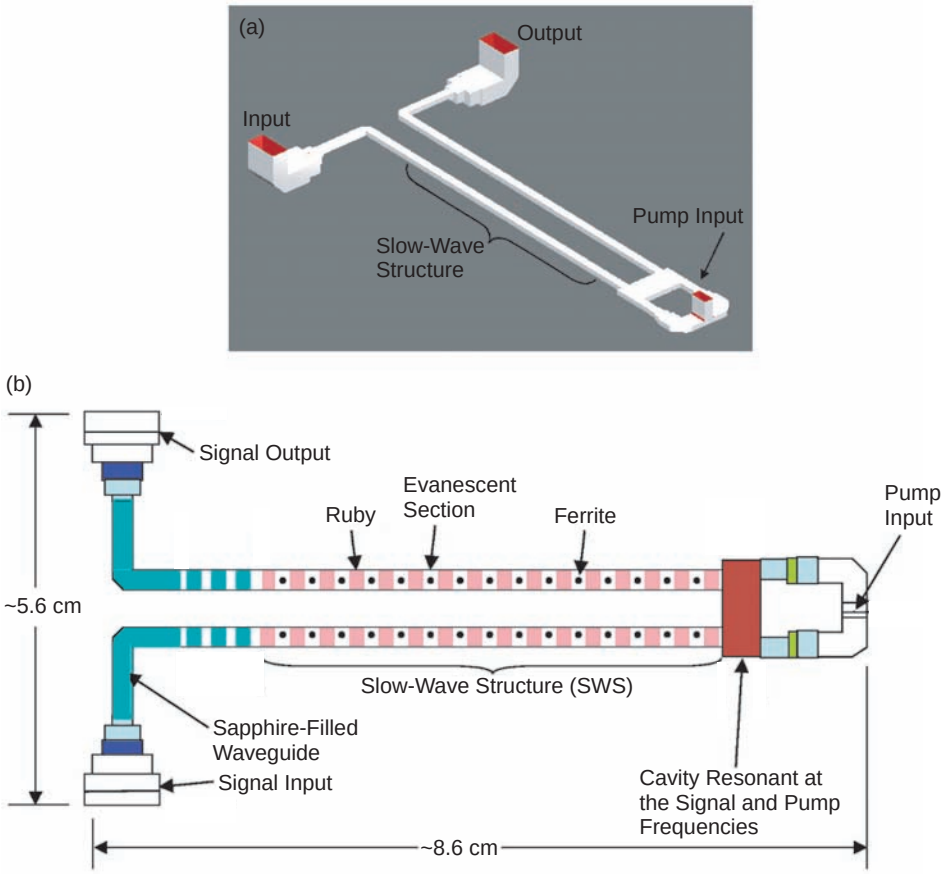

Fig. 3-21. 32 GHz cascaded-cavity TWM with (a) perspective view and (b) schematic view (not to scale).

feature of this design is the smooth waveguide structure that contains the ruby resonators, without irises. Sections of waveguide containing resonance isolators and a low dielectric constant material are beyond cut-off at the signal frequency and the pump frequency. The ruby resonator dimensions are such that the resonators form a slow-wave structure with pass-bands that exist at both the signal frequency and the pump frequency. This is done to maximize the pumping efficiency, as well as the signal frequency gain-bandwidth product. A "U-turn" cavity is used at one end of the structure enabling the introduction of pump power at that end. The signal input and output connection of the two side-by-side structures are at the end opposite the U-turn cavity.

The approach of using a smooth waveguide structure without irises was also used to design a coupled-cavity reflection type amplifier. A sketch of this design is shown in Fig. 3-22. The cavity closest to the circulator is made of sapphire and serves as a coupling cavity for the signal. Its dimensions are such

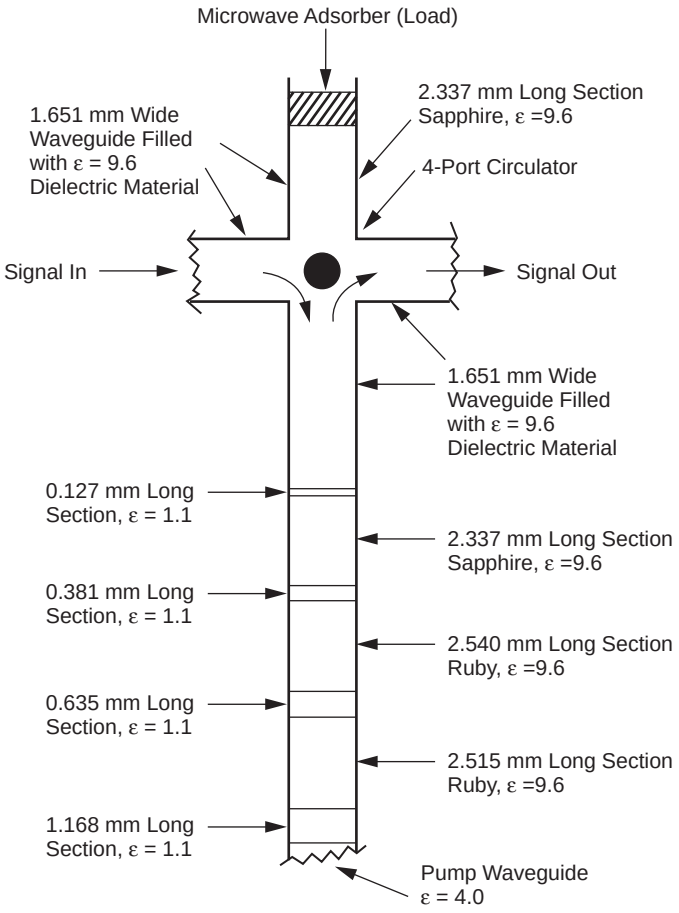

Fig. 3-22. 32-GHz coupled-cavity reflection-type amplifier.

that it reflects pump power, maximizing the pumping efficiency. The following two cavities are ruby and are resonant at both the signal and pump frequencies. Analysis of the coupled-cavity stage shows about 10 dB gain with a 500-MHz bandwidth from 31.8 GHz to 32.3 GHz when cooled to 1.5 K. Four stages can be used in series to produce 40 dB gain with a 500-MHz bandwidth. The analyzed frequency response for the four-stage smooth-wall coupled-cavity maser is shown in Fig. 3-23.

The simple coupled-cavity maser design is also well suited for laboratory measurements requiring the ultimate sensitivity. Calculations of the coupled-cavity maser noise temperature show effective input noise temperatures of 1.983 K when cooled to 1.0 K, 2.343 K when cooled to 1.5 K, 2.573 K when cooled to 1.8 K, and 2.754 K when cooled to 2.0 K. Connected to a termination in the super-fluid helium bath, the total operating system noise temperatures would be 2.404 K, 3.204 K, 3.713 K, and 4.083 K at bath temperatures of 1.0 K, 1.5 K, 1.8 K, and 2.0 K, respectively. The h*f*/k quantum noise at 32 GHz is 1.536 K, which represents 63.9 percent of the total system temperature in the 1.0-K bath and 37.6 percent of the total system temperature in the 2.0-K bath. Laboratory measurements verifying the thermal and quantum noise temperature quantities are suggested.

These ruby maser designs are available for future applications when stringent deep space telecommunications link needs arise at 32 GHz, as they have historically at S-band and X-band.

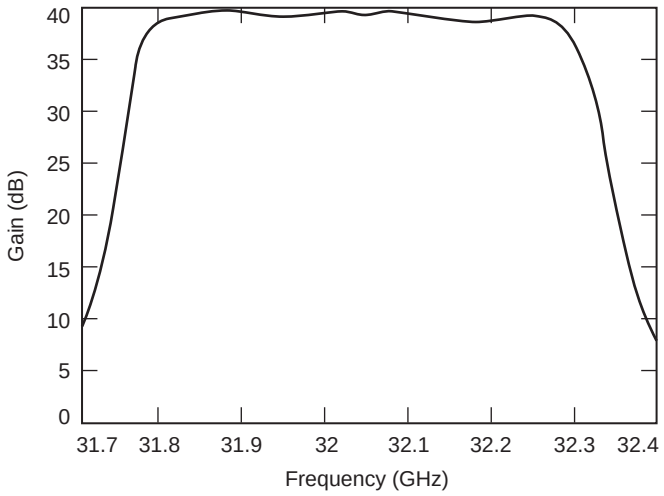

Fig. 3-23. Analyzed frequency response of four-stage 32-GHz coupled cavity reflection-type amplifier.

References

[1] W. R. Corliss, *A History of the Deep Space Network*, NASA CR-151915, National Aeronautics and Space Administration, Washington, District of Columbia, May 1, 1976.

[2] T. Sato and C. T. Stelzried, "An Operational 960 Mc Maser System for Deep Space Tracking Missions," *IRE Transactions on Space Electronics and Telemetry*, vol. SET-8, pp. 164–170, June 1962.

[3] R. C. Clauss, "A 2388Mc Two-Cavity Maser for Planetary Radar," *Microwave Journal*, vol. 8, pp. 74–77, May 1965.

[4] M. S. Reid, R. C. Clauss, D. A. Bathker, and C. T. Stelzried, "Low-Noise Microwave Receiving Systems In A Worldwide Network of Large Antennas," *Proceedings of the IEEE*, vol. 61, pp. 1330–1335, 1973.

[5] J. S. Shell, R. C. Clauss, S. M. Petty, G. W. Glass, M. S. Fiore, J. J. Kovatch, J. R. Loreman, D. E. Neff, R. B. Quinn, and D. L. Trowbridge, "Ruby Masers for Maximum G/T_{op}," *Proceedings of the IEEE*, vol. 82, no. 5, pp. 796–810, May 1994.

[6] A. E. Siegman, *Microwave Solid State Masers*, McGraw-Hill Book Company, New York, New York, 1964.

[7] W. S. Chang and A. E. Siegman, *Characteristics of Ruby for Maser Applications*, Tech. Rept. 156-2 Stanford Electronics Laboratories, Stanford University, California, September 30, 1958.

[8] A. R. Kerr, "Suggestions for Revised Definitions of Noise Quantities, Including Quantum Effects," *IEEE Transactions on Microwave Theory and Techniques*, vol. 47, no. 3, pp. 325–329, March 1999.

[9] C. T. Stelzried, R. C. Clauss, and S. M. Petty, "DSN Receiving Systems' Operating Noise Temperature Measurements," *The Interplanetary Network Progress Report 42-154, April–June 2003*, Jet Propulsion Laboratory, Pasadena, California, pp. 1–7, August 15, 2003. http://ipnpr.jpl.nasa.gov/progress_report/

[10] R. Clauss and E. Wiebe, "Low-Noise Receivers: Microwave Maser Development," *The Deep Space Network Progress Report for November and December 1973*, Technical Report 32-1526, Vol. XIX, Jet Propulsion Laboratory, Pasadena, California, pp. 93–98, February 15, 1974. http://ipnpr.jpl.nasa.gov/progress_report/

[11] R.W. DeGrasse, E. O.Schulz-DuBois, H. E. D. Scovil, "The Three-Level Solid State Traveling Wave Maser," *The Bell System Technical Journal*, vol. 38, no. 2, pp. 305–334, March 1959.

[12] S. Okwit, F. R. Arams, and J. G. Smith, "Electronically Tunable Traveling-Wave Masers at L and S-Bands," *Proceedings of the IRE*, vol. 48, p. 2025, May 1960.

[13] D. L Trowbridge, "Block III Maser Implementation Program," *The Deep Space Network Progress Report for September and October 1973*, Technical Report 32-1526 Vol. XVIII, Jet Propulsion Laboratory, Pasadena, California, pp.130–135, December 15, 1973. http://ipnpr.jpl.nasa.gov/progress_report/

[14] J. W. Layland, "ICE Telemetry Performance," *The Telecommunications and Data Acquisition Progress Report 42-84, October–December 1985*, Jet Propulsion Laboratory, Pasadena, California, pp. 203–213, February 15, 1986. http://ipnpr.jpl.nasa.gov/progress_report/

[15] J. W. Layland and L. L. Rauch, "The Evolution of Technology in the Deep Space network: A History of the Advanced Systems Program," *The Telecommunications and Data Acquisition Progress Report 42-130, April–June 1997*, Jet Propulsion Laboratory, Pasadena, California, pp. 1–44, August 15, 1997. http://ipnpr.jpl.nasa.gov/progress_report/

[16] C. T. Stelzried, "Operational Performance of an H-Band Coupled Cavity Transmission Maser," *Microwave Journal*, vol. 10, pp. 103–106, March 1967.

[17] S. M. Petty and R. C. Clauss, "X-Band Traveling Wave Maser," *IEEE Transactions on Microwave Theory and Technology*, vol. MTT-16, no. 1, pp. 47–48, January 1968.

[18] R. Berwin, E. Wiebe, and P. Dachel, "Superconducting Magnet for a Ku-Band Maser," *The Deep Space Network Progress Report for July and August 1971*, Technical Report 32-1526, Vol. V, Jet Propulsion Laboratory, Pasadena, California, pp. 109–114, October 15, 1971. http://ipnpr.jpl.nasa.gov/progress_report/

[19] R. Clauss and R. Quinn, "Low Noise Receivers, Microwave Maser Development," *The Deep Space Network Progress Report for July and August 1971*, Technical Report 32-1526, Vol. V, Jet Propulsion Laboratory, Pasadena, California, pp. 102–108, October 15, 1971. http://ipnpr.jpl.nasa.gov/progress_report/

[20] R. W. Berwin, *Paramagnetic Energy Levels of the Ground State of Cr^{+3} in Al_2O_3 (Ruby)*, JPL Technical memorandum 33-440, Jet Propulsion Laboratory, Pasadena, California, January 15, 1970.

[21] C. R. Moore and R. C. Clauss, "A Reflected-Wave Ruby Maser with K-band Tuning Range and Large Instantaneous Bandwidth," *IEEE Transactions on Microwave Theory and Techniques*, vol. MTT-27, no. 3, pp. 249–256, March 1979.

[22] D. L. Trowbridge, "X-Band Traveling Wave Maser Amplifier," *The Deep Space Network Progress Report for July and August 1973*, Technical Report 32-1526 Vol. XVII, Jet Propulsion Laboratory, Pasadena, California, pp. 123–130, October 15, 1973. http://ipnpr.jpl.nasa.gov/progress_report/

[23] D. L. Trowbridge, "X-band, Low-Noise, Traveling-Wave Maser," *The Telecommunications and Data Acquisition Progress Report 42-60, September and October 1980*, Jet Propulsion Laboratory, Pasadena, California, pp. 1–38, pp. 126–132, December 15, 1980. http://ipnpr.jpl.nasa.gov/progress_report/

[24] R. C. Clauss and R. B. Quinn, *Resonant Isolator for Maser Amplifier*, New Technology Transmittal NASA-CASE-NPO-15201-1 (NASA-15201), National Aeronautics and Space Administration, Pasadena Office, Pasadena, California, 1983.

[25] D. L. Johnson, S. M. Petty, J. J. Kovatch, and G. W. Glass, "Ultralow Noise Performance of an 8.4-GHz Maser–Feedhorn System," *The Telecommunications and Data Acquisition Progress Report 42-100, October–December 1990*, Jet Propulsion Laboratory, Pasadena, California, pp. 100–110, February 15, 1990. http://ipnpr.jpl.nasa.gov/progress_report/

[26] R. C. Clauss, "Low Noise Receivers: Microwave Maser Development," *The Deep Space Network Progress Report 42-25, November and December 1974*, Jet Propulsion Laboratory, Pasadena, California, pp. 65–68, February 15, 1975. http://ipnpr.jpl.nasa.gov/progress_report/

[27] L. D. Flesner and Sheldon Schultz, "Simple Waveguide Reflection Maser with Broad- Tunability," *Review of Scientific Instruments*, vol. 48, no. 8, pp. 1104–1105, August 1977.

[28] C. R. Moore, "A K-Band Ruby Maser with 500-MHz Bandwidth," *IEEE Transactions on Microwave Theory Techniques*, vol. MTT-28, no. 2, pp. 149–151, February 1980.

[29] J. Shell and D. Neff, "A 32 GHz Reflected Wave Maser Amplifier with Wide Instantaneous Bandwidth," *1988 MTTS International Microwave Symposium Digest* (1988 Vol. II [MYSYM]), pp. 789–792, 1988.

[30] *WASP-NET, Waveguide Synthesis Program for Waveguide Networks*, Microwave Innovation Group, Bremen, Germany.

[31] G. L. James, "Analysis and Design of TE_{11}-to-HE_{11} Corrugated Cylindrical Waveguide Mode Converters," *IEEE Transactions on Microwave Theory and Techniques*, MTT-29, no. 10, pp. 1059–1066, October 1981.

[32] D. J. Hoppe, "Modal Analysis Applied to Circular, Rectangular, and Coaxial Waveguides," *The Telecommunications and Data Acquisition Progress Report 42-95, July–September 1988*, Jet Propulsion Laboratory, Pasadena, California, pp. 89–96, November 15, 1988. http://ipnpr.jpl.nasa.gov/progress_report/

[33] B. Lax and K. J. Button, *Microwave Ferrites and Ferrimagnetics*, McGraw-Hill Book Co., New York, New York, 1962

[34] A. Abragam and B. Bleaney, *Electron Paramagnetic Resonance of Transition Ions*, Dover Publications, Inc., New York, New York, 1986.

[35] E. O. Schulz-DuBois, "Paramagnetic Spectra of Substituted Sapphires-Part I: Ruby," *Bell System Technical Journal*, vol. 38, pp. 271–290, January 1959.

[36] T. Chang, D. Foster, and A. H. Kahn, "An Intensity Standard for Electron Paramagnetic Resonance Using Chromium-Doped Corundum (Al_2O_3:Cr^{3+})," *Journal of Research of the National Bureau of Standards*, vol. 83, no. 2, pp. 133–164, March–April 1978.

[37] J. S. Shell and R. C. Clauss, "A 32 GHz Coupled Cavity Maser Design," *The Telecommunications and Mission Operations Progress Report 42-142, April–June 2000*, Jet Propulsion Laboratory, Pasadena, California, pp. 1–22, August 15, 2000. http://ipnpr.jpl.nasa.gov/progress_report/

[38] J. Shell and R. Clauss, "A 32-Gigahertz Traveling-Wave Maser Design," *The Interplanetary Network Progress Report 42-159*, Jet Propulsion Laboratory, Pasadena, California, pp. 1–22, November 15, 2004. http://ipnpr.jpl.nasa.gov/progress_report/

[39] J. C. Fletcher and E. R. Wiebe, *Multistation Refrigeration System*, United States Patent 4,077,231, March 7, 1978.

[40] J. C. Fletcher and E. R. Wiebe, *Helium Refrigerator*, United States Patent 3,914,950, October 28, 1975.

[41] J. C. Fletcher, E. R. Wiebe, and R. C. Clauss, *Refrigerated Coaxial Coupling*, United States Patent 3,902,143, August 26, 1975.

[42] G. M. Low and E. R. Wiebe, *Helium Refrigerator and Method for Decontaminating the Refrigerator*, United States Patent 3,656,313, April 18, 1972.

[43] E. R. Wiebe, *Closed-Cycle Refrigerator for Masers*, NPO-13839 (NASA Technical Reports Server Document ID 19770000056), Jet Propulsion Laboratory, Pasadena, California, 1977.

[44] E. R. Wiebe, *Measuring Cryogenic-Refrigerator Cooling Capacity*, NPO-13435 (NASA Technical Reports Server Document ID 19770000411), Jet Propulsion Laboratory, Pasadena, California, 1978.

[45] E. R. Wiebe, *Automatic Thermal Switch Accelerates Cooling-Down of Cryogenic System* (NASA Technical Reports Server Document ID 195650000067), Jet Propulsion Laboratory, Pasadena, California, 1965.

[46] W. Higa and E. R. Wiebe, *Spiraled Channels Improve Heat Transfer Between Fluids* (NASA Technical Reports Server Document ID 119650000289, Jet Propulsion Laboratory, Pasadena, California, 1965.

[47] R. C. Clauss, *Transmission Line Thermal Short*, United States Patent 3,474,357, October 21, 1969.

[48] T. O. Paine and R. C. Clauss, *High-Gain Broadband Traveling Wave Maser*, United States Patent 3,486,123, December 23, 1969.

[49] G. M. Low, R. B. Quinn, and R. C. Clauss, *Maser for Frequencies in the 7-20 GHz Range*, United States Patent 3,676,787, July 11, 1972.

[50] J. C. Fletcher and R. C. Clauss, *Reflected-Wave Maser*, United States Patent 3,978,417, August 31, 1976.

[51] J. C. Fletcher, E. R. Wiebe, and R. C. Clauss, *Refrigerated Coaxial Coupling*, United States Patent 3,902,143, August 26, 1975.

[52] R. A. Frosch, R. C. Clauss, and R. B. Quinn, *Dielectric-Loaded Waveguide Circulator for Cryogenically Cooled and Cascaded Maser Waveguide Structures*, United States Patent 4,187,470, February 5, 1980.

[53] R. C. Clauss and R. B. Quinn, *Resonant Isolator for Maser Amplifier*, United States Patent 4,399,415, August 16, 1983.